5-2012

Active Neutron Interrogation of Non-Radiological Materials with the Nuclear Materials Identification System

Mark Edwin Walker
mwalke51@utk.edu

John T. Mihalczo
Oak Ridge National Laboratory, 6jt@ornl.gov

OAK RIDGE
NATIONAL LABORATORY
MANAGED BY UT-BATTELLE
FOR THE DEPARTMENT OF ENERGY

ORNL/TM-2012/77

Active Neutron Interrogation of Non-Radiological Materials with the Nuclear Materials Identification System

February 2012

Prepared by

Mark E. Walker
John T. Mihalczo

UT-BATTELLE
ORNL-27 (4-00)

ORNL/TM-2012/77

Global Nuclear Security Technology Division

ACTIVE NEUTRON INTERROGATION OF NON-RADIOLOGICAL MATERIALS WITH THE NUCLEAR MATERIALS IDENTIFICATION SYSTEM

Mark E. Walker, The University of Tennessee, Knoxville
John T. Mihalczo, Oak Ridge National Laboratory

Date Published: February 2012

Prepared by
OAK RIDGE NATIONAL LABORATORY
Oak Ridge, Tennessee 37831-6283
managed by
UT-BATTELLE, LLC
for the
U.S. DEPARTMENT OF ENERGY
under contract DE-AC05-00OR22725

CONTENTS

Page

LIST OF FIGURES

Figure **Page**

LIST OF TABLES

Table **Page**

ABSTRACT

The Nuclear Materials Identification System (NMIS) at Oak Ridge National Laboratory (ORNL), although primarily designed for analyzing special nuclear material, is capable of identifying non-radiological materials with a wide range of measurement techniques. This report demonstrates four different measurement methods, complementary to fast-neutron imaging, which can be used for material identification: DT transmission, DT scattering, californium transmission, and active time-tagged gamma spectroscopy. Each of the four techniques was used to evaluate how these methods can be used to identify four materials: aluminum, polyethylene, graphite, and G-10 epoxy. While such measurements have been performed individually in the past, in this project, all four measurements were performed on the same set of materials. The results of these measurements agree well with predicted results. In particular, the results of the active gamma spectroscopy measurements demonstrate the technique's applicability in a future version of NMIS which will incorporate passive and active gamma-ray spectroscopy. This system, designated as a fieldable NMIS (FNMIS), is under development by the US Department of Energy Office of Nuclear Verification.

1. INTRODUCTION

A wide range of measurement techniques can be used in conjunction with the Nuclear Materials Identification System (NMIS) (Mattingly et al., 2000) fast-neutron imaging to accurately characterize nonradiological materials. This paper demonstrates applications of the following four measurement methods that are useful in material identification with NMIS-type measurements.

1. **Deuterium-Tritium** (**DT) Neutron Transmission**: Time-of-flight transmission measurements of 14.1 MeV neutrons through an object

2. **DT Neutron Scattering**: Time-of -flight measurements of 14.1 MeV neutron reflection

3. **Californium Neutron Transmission**: Time-of-flight transmission measurements of fission spectrum neutrons from a ^{252}Cf source

4. **Active Gamma Spectroscopy**: Measurements of time-tagged gamma-ray emissions from non-elastic neutron interactions

DT transmission, DT scattering, and californium transmission have been demonstrated in previous papers (Grogan et al., 2008; Mihalczo et al., 2000). Active gamma spectroscopy has been proposed for NMIS (Mihalczo et al., 2004) and has been used for explosive (Hurley and Tinsley, 2007). A future fieldable version of NMIS is under development by the US Department of Energy Office of Nuclear Verification (ONV) for possible use in future treaty applications. This system (Radle et al., 2009; Mihalczo et al., 2010) will eventually incorporate passive and active gamma-ray spectroscopy using HPGe scintillator detectors.

This paper presents measurements using these four techniques with aluminum, polyethylene (C_2H_4), graphite (elemental carbon), and G-10 epoxy, which contains carbon, hydrogen, oxygen, and nitrogen, and shows how these methods can complement fast-neutron imaging to assist in material identification. These methods may be particularly useful for identifying materials with the similar fast-neutron transmission properties, which are difficult to differentiate in a fast-neutron imaging measurement.

2. NMIS CONCEPTS

NMIS is a time-dependent coincidence counting system that is used to characterize both fissile and non-fissile materials undergoing nondestructive assay (Chiang et al., 2001). NMIS characterizes materials by interrogating them with neutrons, either from an associated-particle DT neutron generator, which produces 14.1 MeV neutrons, or from a californium-252 spontaneous fission source, which produces a distribution of neutrons ranging from approximately 0.2 MeV to 7 MeV (Smith et al., 1957). NMIS has also been used with pulsed neutron sources, including a deuterium-deuterium (DD) generator and a linear accelerator (McConchie et al., 2009; Mihalczo, 2004). The system has also been used for passive measurements on materials with inherent neutron sources, such as ^{240}Pu (Pozzi et al., 2005). The DT generator produces neutrons by accelerating deuterium and tritium molecules into a metal hydride target, which also contains deuterium and tritium. The resulting fusion reaction between deuterium and tritium produces an alpha particle and a 14.1 MeV neutron, which are emitted in essentially opposite directions. Embedded in the generator is a scintillator adjacent to a fiber-optic face plate, whose outside face is adjacent to a pixelated light guide. The light guide is adjacent to a pixelated photomultiplier tube (PMT). This setup, documented in Fig. 1, allows time and direction tagging of neutrons produced by the generator, through the detection of their associated alpha particles.

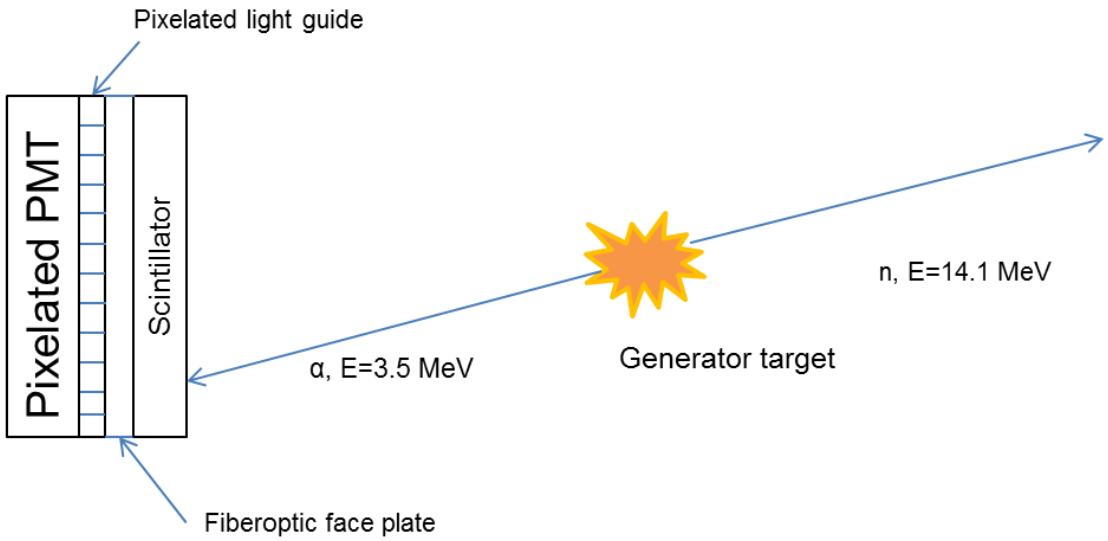

Fig. 1. Schematic of particle generation and tagging in an associated particle DT generator (not to scale).

The californium-252 source time-tags neutrons by producing a pulse when a fission event occurs inside a parallel plate ion chamber. Californium is deposited on one plate in the chamber, so that each spontaneous fission event ionizes the gas inside, producing a timing pulse.

Tagged neutrons, from either the DT source or the californium source, subsequently interact with the object that is being interrogated. Neutrons that are transmitted through the object, as well as products of neutron interactions inside the object, are detected in a horizontal fan array of 32 sequentially numbered plastic scintillators. A schematic of possible neutron interactions through an object is displayed in Fig. 2, and, for reference, a picture of NMIS is shown in Fig. 3.

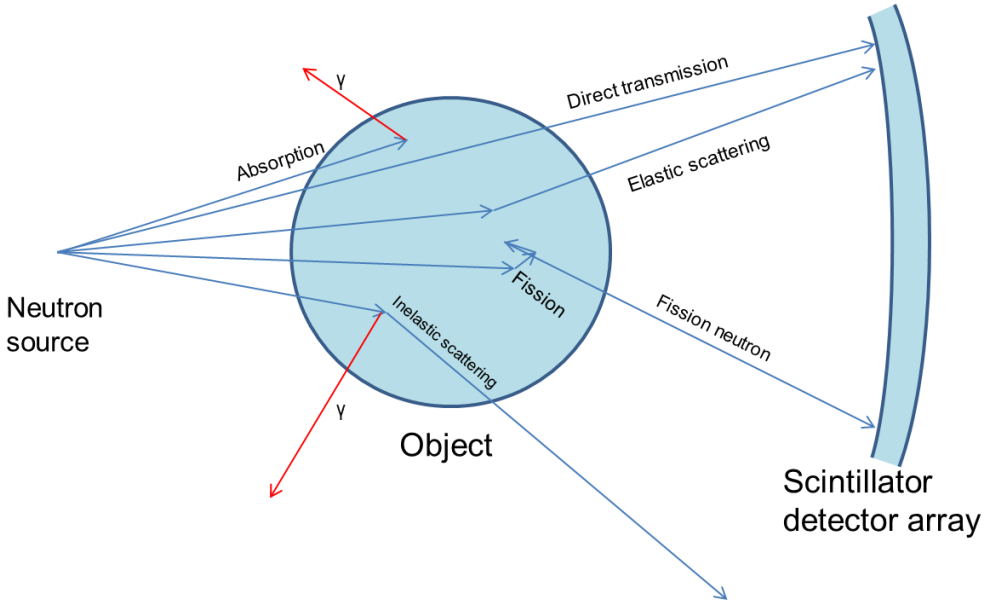

Fig. 2. Schematic of a transmission measurement with NMIS.

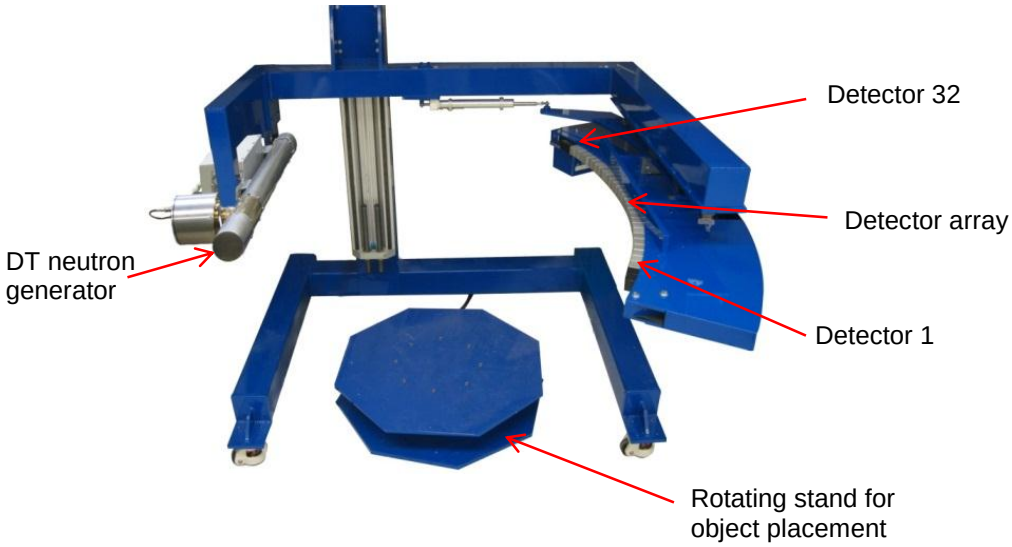

Fig. 3. Photograph of NMIS with a DT generator in use as a neutron source.

Signals from either the alpha pixels in the DT generator or the californium source are processed through constant fraction discriminators (CFDs), along with signals from the plastic scintillator array. Pulses from the CFDs are transmitted to a 10 channel, 1 GHz processor (Mihalczo et. al, 2000) which analyzes coincident pulses between the detectors. Many detectors can be input to the same processor channel if they have different pulse widths, since the processor identifies pulses according to their width within the same channel of the processor. This data can then be used to trace the paths of neutrons through the object being measured. When a DT generator is being used, data from NMIS can be used to produce a horizontal cross-sectional image of an object, mapped by 14 MeV neutron attenuation coefficients (Mullens et al., 2004). NMIS can be also configured to measure the spatial distribution of fission inside the object (Hausladen et al., 2006).

3. DT TRANSMISSION

In a DT transmission measurement, a monoenergetic beam of 14.1 MeV neutrons is transmitted through a material. The beam is used to measure the material's neutron attenuation properties, which can aid in its identification. This section shows how a material's neutron attenuation characteristics can be measured.

3.1 EXPERIMENTAL SETUP

For this series of measurements, a DT neutron generator (Thermo-Fisher API-120) was used as the neutron source. Alpha particles originating from the 5-mm-diameter target spot were detected with a YAP:Ce scintillator. A pixelated photomultiplier tube (Hamamatsu H9500) divided the light from the scintillator into 16 horizontal pixels, with a total width of 48 mm and a height of 3 mm. The tagged neutron cones cover a horizontal angle of approximately 45°, and a vertical angle of approximately 3.5°. Material samples were placed on a 40.5° angle to the generator's long axis, and the face of each sample was 51 cm away from the generator target, along the long axis. This setup is shown in Fig. 4.

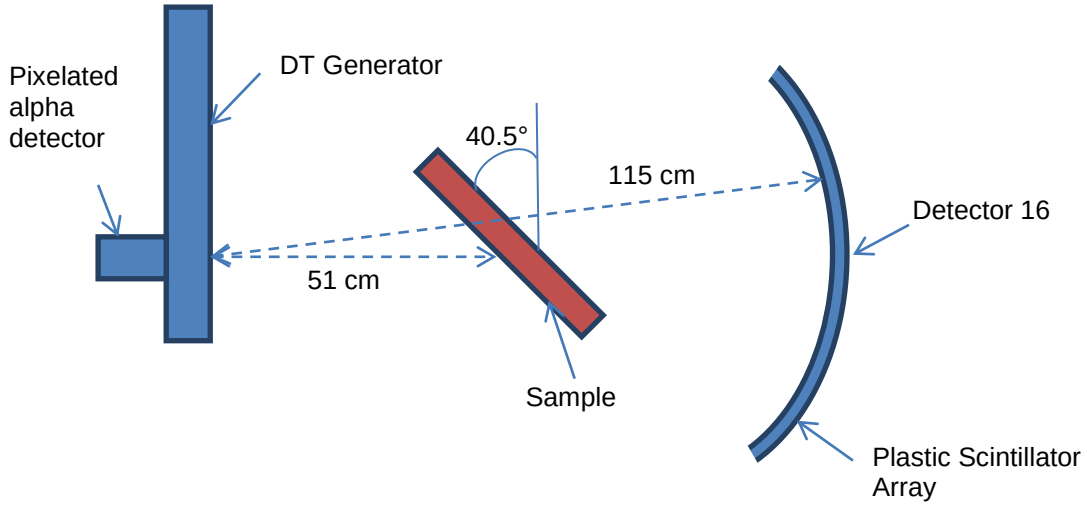

Fig. 4. Experimental setup for DT transmission measurements (not to scale).

The detector array shown on the right side of Fig. 4 consisted of thirty-two 2.5×2.5×10.2 cm plastic scintillator detectors (Scionix Holland V25.4B102/1-E1-PXNEG). The array was arranged in an arc so that each detector was 115 cm away from the neutron generator's target. The middle of the generator and the detectors were 113 cm above the floor.

Signals from the alpha detector and the plastic scintillators were processed through constant fraction discriminators (ORTEC 935 and ORTEC CF 8000, respectively), and subsequently through the NMIS processor (Mihalczo et al., 2000). Time correlations between events in the alpha detector and events in the plastic scintillator array were measured, with an overall timing uncertainty of ±1 ns.

For each measurement, the neutron generator was operated at 25 μA of beam current and 75 kV of high voltage. Measurement times were 42.7 minutes for each sample, and an additional 8.5 minute measurement was performed with no sample present.

The physical characteristics of the material samples used in the DT transmission experiment are shown in Table 1.

Table 1. Properties of materials used in DT transmission measurements

Material	Dimensions (cm)	Weight (kg)	Density (g/cm^3)
Polyethylene	30.5×30.5×3.8	3.329 ± 0.001	0.94
Aluminum	30.5×30.5×3.8	9.263 ± 0.001	2.62
Graphite	45.7×45.7×7.6	27.895 ± 0.001	1.76
G-10	30.5×30.5×2.5	4.674 ± 0.001	2.01

3.2 THEORY

The neutron attenuation properties for each of the material samples were obtained from time-correlation spectra between alpha pixel 8 and detector 16 in the scintillator array. An example of a time-correlation spectrum is shown in Fig. 5. The peak in the spectrum occurs at ~22 ns because 14.1 MeV neutrons, travelling at 5.1 cm/ns, take approximately 22 ns to traverse the 115 cm distance between the neutron generator and the plastic scintillator array.

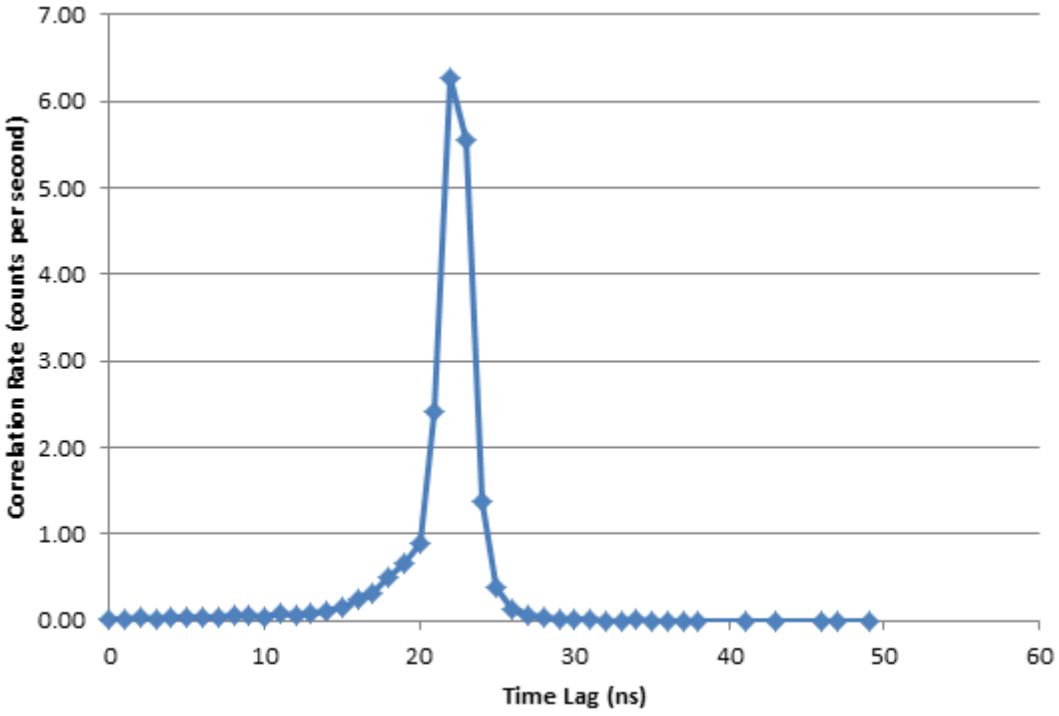

Fig. 5. Time-correlation spectrum for a void measurement between pixel 8 and imaging detector 16.

Neutron attenuation was calculated using the following relationship:

$$Attenuation = -\ln\left(\frac{I_{sample}}{I_{void}}\right), \quad (1)$$

where I_{sample} is the neutron correlation rate in the transmission peak between a pixel to a plastic detector with a material sample present, and I_{void} is the neutron correlation rate between the same pixel to the same plastic detector with no sample present. The number of neutrons transmitted in each case was calculated by integrating the peak of the time-correlation spectrum between -4 ns to +3 ns with respect to the maximum of the curve. The calculated attenuation of each material sample was compared to a benchmark value, given by the equation

$$Attenuation = \Sigma_{tot} x, \quad (2)$$

where Σ_{tot} is the total macroscopic neutron cross section of the material for 14.1 MeV neutrons, and x is the neutron path length through the material. Macroscopic neutron cross-section values were derived from microscopic neutron cross-section data found in the ENDF/B-VII.1 database (Chadwick et al., 2011).

3.3 RESULTS AND DISCUSSION

The expected and observed attenuations for pixel 8 and imaging detector 16 are shown in Table 2. The values for nuclear density, microscopic cross section (σ_{tot}), and macroscopic cross section (Σ_{tot}) for G10 epoxy are not shown because its chemical formula is proprietary to the material's vendor.

Table 2. Measured sample attenuation for pixel 8 and imaging detector 16

Material	Density (g/cc)	Nuclear density (nuclei/ barn-cm)	σ_{tot} @ 14.1 MeV (barns)	Σ_{tot} (cm^{-1})	Neutron path length (cm)	Expected attenuation	Measured attenuation
Aluminum	**2.62**	**0.058**	**1.75**	**0.102**	**5.00**	**0.51**	**0.48**
Polyethylene	**0.94**	**0.121**		**0.109**	**5.00**	**0.54**	**0.54**
C		0.040	1.32	0.053			
H		0.081	0.68	0.055			
Graphite	**1.75**	**0.088**	**1.32**	**0.116**	**9.99**	**1.16**	**1.13**
G10 Epoxy	**2.01**	**N/A**	**N/A**	**N/A**	**3.29**	**N/A**	**0.37**

The measured attenuation values are very consistent with the values predicted using ENDF data. Attenuation values for aluminum and carbon were underestimated because of neutrons that scattered in the forward direction and lost very little energy. These neutrons are difficult to differentiate from transmitted neutrons, since both transmitted and forward scattered neutrons arrive in the plastic scintillator detectors at the same time. Neutrons tend to scatter forward in interactions with heavier nuclei. It follows that the largest fractional error, at 5.9%, is for the aluminum sample, which contains the heaviest nuclei. The measured attenuation for the carbon sample only deviates from the expected value by 2.6%, since forward scattering tends to occur less in carbon, due to its smaller nuclear mass.

A scattering correction can be made to compensate for forward neutron scattering (Grogan, 2010) but was not carried out on this set of measurements. While a scattering correction would improve the accuracy of the aluminum neutron attenuation value, it would worsen the polyethylene attenuation value, because very little forward neutron scattering occurs inside polyethylene.

The macroscopic cross section of the G10 Epoxy sample, obtained from its measured attenuation, was 0.112 cm^{-1}, which is similar to the macroscopic cross sections of carbon, polyethylene, and aluminum given in Table 2. DT transmission measurements can provide useful information about an unknown material. Many materials, however, share very similar neutron attenuation properties. Aluminum and polyethylene, for example, have nearly identical macroscopic neutron cross sections at 14 MeV. Therefore, additional measurement techniques are often necessary for the accurate characterization of some materials.

4. DT SCATTERING

Time-of-flight measurements of elastically scattered neutrons along a known trajectory can be useful in identifying the nuclear mass of an unknown material. This section demonstrates the viability of performing time-of-flight scattering measurements with NMIS system and how this measurement method can aid in the identification of materials.

4.1 EXPERIMENTAL SETUP

DT scattering measurements used the same setup as the DT transmission measurements previously presented in this paper but also made use of four 9.5×9.5×10.1 cm plastic scintillator detectors (Bicron 3.75×3.75H4BC420/3L) placed outside of the neutron cone defined by pixel 10 to count elastically scattered neutrons, as well as the time distribution of gamma rays originating from non-elastic neutron interactions. For this series of measurements, pulses in the scattering detectors were correlated with pixel 10 in the generator. The detectors were placed side by side in an array perpendicular to the long axis of the neutron generator, and each was shielded in a 6-mm-thick lead on the front and sides, to reduce counts from gamma rays produced by non-elastic neutron scattering. The scattering detectors were assigned sequential numbers, such that detector 1 was furthest away from the DT generator, and detector 4 was closest to the generator. The face of detector 1 was 78 cm from the surface of the material sample in the path of the neutron beam from pixel 10.

The horizontal centerline of the detectors was 113 cm above the floor, at the same height as the detector array used for the DT transmission measurements. A 10.4×10.4×10.4 cm tungsten block was placed between the DT generator and scattering detectors to shield the array from neutrons directly transmitted from the generator. A schematic of this setup is shown in Fig. 6.

The physical properties of the material samples used for this series of experiments are exactly the same as those shown in Table 1.

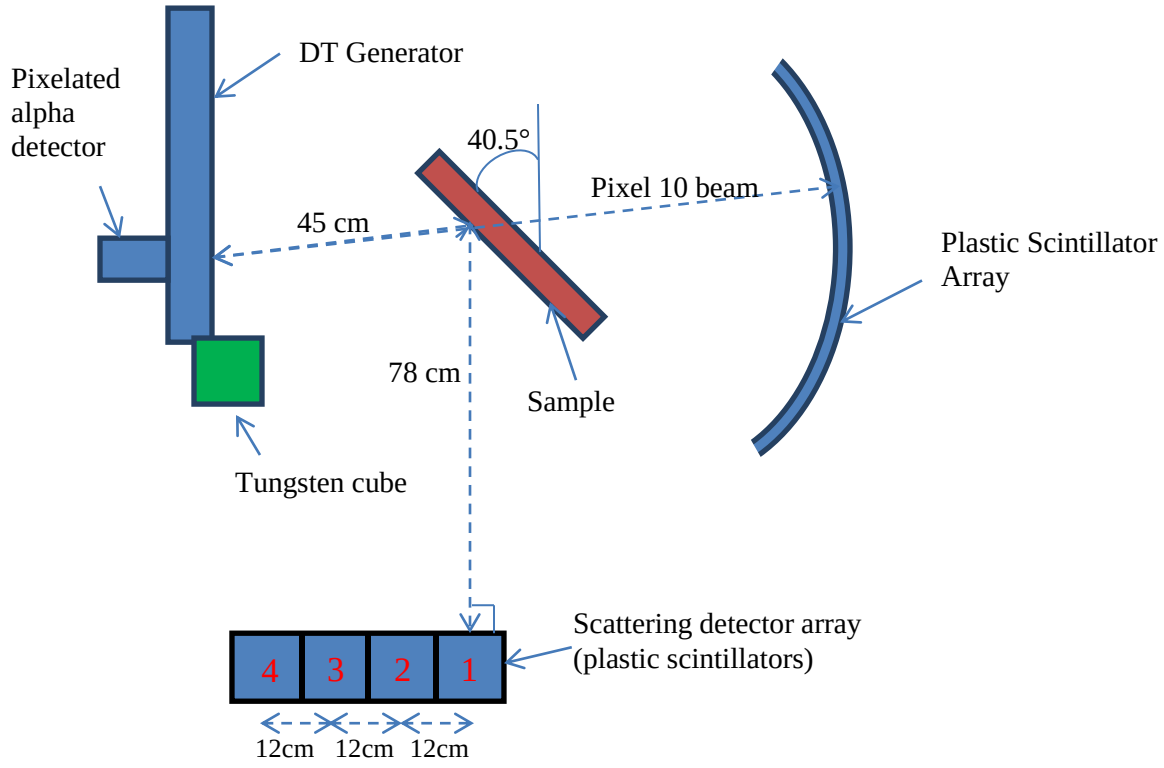

Fig. 6. Experimental setup for DT scattering experiment (not to scale).

The scattering angles required for neutrons to reach the four scattering detectors are shown in Table 3, along with the distances from the sample to each detector. As in the DT transmission measurement, the neutron generator was operated at 25 μA of beam current and 75 kV of high voltage. The duration of each measurement was 42.7 minutes.

Table 3. Reference positions for scattering detector array

Detector number	Scattering angle from sample (degrees)	Distance from sample to detector (cm)
1	99	78
2	108	78.9
3	117	81.6
4	127	85.9

Time-of-flight scattering measurements were performed by correlating counts recorded in pixel 10 with pulses from the four scattering detectors.

4.2 THEORY

The arrival time of elastically scattered neutrons in each of the four scattering detectors is equal to the sum of two values:

1. the time it takes for a 14.1 MeV neutron to travel to the sample, and
2. the time it takes for the scattered neutron to travel from the sample to the detector.

The distance from the generator to the sample, along the beam of pixel 10, was measured to be 45 cm. Since 14.1 MeV neutrons travel at 5.14 cm/ns, it takes 8.8 ns for the neutrons to reach the sample from the generator.

The time-of-flight of scattered neutrons from the sample to the detectors depends on the distance from the sample to the detectors, as well as the energy of the scattered neutrons which is given by (Duderstadt and Hamilton, 1976):

$$E_f = \frac{1}{2}[1 + \alpha + (1 - \alpha)cos\theta_{cm}]E_i \,, \tag{3}$$

where E_f is the final energy of the scattered neutron, E_i is the initial energy of the neutron, θ_{cm} is the neutron scattering angle in the center-of-mass reference frame, and α is a constant related to the target nucleus's atomic mass, *A*, where

$$\alpha = \left(\frac{A-1}{A+1}\right)^2 . \tag{4}$$

Thus, the final energy of the scattered neutron is dependent upon the angle of scattering and the mass of the target nucleus.

For this experiment, it is safe to assume that θ_{cm} is equal to the neutron scattering angle in the laboratory reference frame (given in Table 3), and nuclei such as carbon and aluminum are relatively large compared to a neutron and gain very little recoil energy from scattering interactions.

Gamma rays originating from non-elastic neutron interactions in the sample also travel to the scattering detectors but arrive much sooner than the neutrons, since gamma rays travel at 30 cm/ns. The expected arrival times in each of the four detectors, calculated with Equations (3) and (4), are shown in Tables 4 and 5 for graphite, polyethylene, and aluminum samples. Neutrons are expected to arrive sooner in the aluminum measurement than in the graphite measurement because neutrons tend to retain more energy when scattering from heavier nuclei for a given scattering angle.

Table 4. Expected neutron and gamma arrival times for a graphite or polyethylene sample

Detector	E_f (MeV)	γ arrival time (ns)	Neutron arrival time (ns)
1	11.8	11.4	25.3
2	11.5	11.4	25.7
3	11.2	11.5	26.5
4	10.9	11.6	27.7

Table 5. Expected neutron and gamma arrival times for an aluminum sample

Detector	E_f (MeV)	γ arrival time (ns)	Neutron arrival time (ns)
1	13.0	11.4	24.5
2	12.8	11.4	24.8
3	12.7	11.5	25.5
4	12.5	11.6	26.5

4.3 RESULTS

Time-of-flight measurements for aluminum, polyethylene, graphite and G-10 epoxy are shown in Figs. 7, 8, 9, and 10, respectively.

In Fig. 7, the peaks that appear at 10 ns are from photons that are produced in the sample from non-elastic neutron interactions. The peaks at ~25 ns are composed of neutrons that elastically scattered in the sample. These peaks are relatively small because aluminum tends to scatter more neutrons in the forward direction. No clear peak is visible at ~25 ns in detector 4, since very few neutrons scatter in the backwards direction. In general, because detector 1 is closest to the object, it covers more solid angle relative to the sample and receives the most counts. Detector 4 receives the least counts, since it covers the least solid angle. A peak near 0 ns is visible in detector 1, which originates from gammas produced by non-elastic neutron interactions in the neutron generator (detector 1 was only partially shielded by the tungsten block).

The basic features of the spectrum in Fig. 8 are the same as those in the aluminum spectrum (Fig. 7). However, the peak at 10 ns is much smaller, because the hydrogen in polyethylene attenuates incoming neutrons, reducing their energy below the threshold required for inelastic scattering from carbon nuclei. Miniature peaks are visible in data from detector 1 at 34 ns and 42 ns, which may originate from inelastic neutron scattering of neutrons from carbon nuclei, or multiple elastic scattering of neutrons from hydrogen nuclei in the sample.

The time-of-flight spectrum for graphite is very different from the polyethylene spectrum (Fig. 9) in that both the peaks at 10 ns and at 25 ns are much larger. This is due to the non-presence of hydrogen in the graphite sample. Without hydrogen in the sample, reflected neutrons have a much greater chance of exiting the sample and reaching the detectors. Also, the lack of hydrogen reduces the attenuation of incoming neutrons, and allows them to scatter inelastically, producing the photons that are visible in the 10 ns peak. The peaks visible at ~30–35 ns are from neutrons that underwent inelastic scattering interactions with carbon nuclei.

The data in this measurement (Fig. 10) are similar to the polyethylene data in the polyethylene measurement. The peaks at 25 ns are similar in amplitude in both measurements, which indicates the presence of hydrogen in the material. The photon peak at 10 ns, however, is much larger for the G-10 sample. The larger photon peak may be due to the presence of nitrogen in the sample, which has a lower threshold energy for inelastic scattering than carbon (ENDF/B-VII.1).

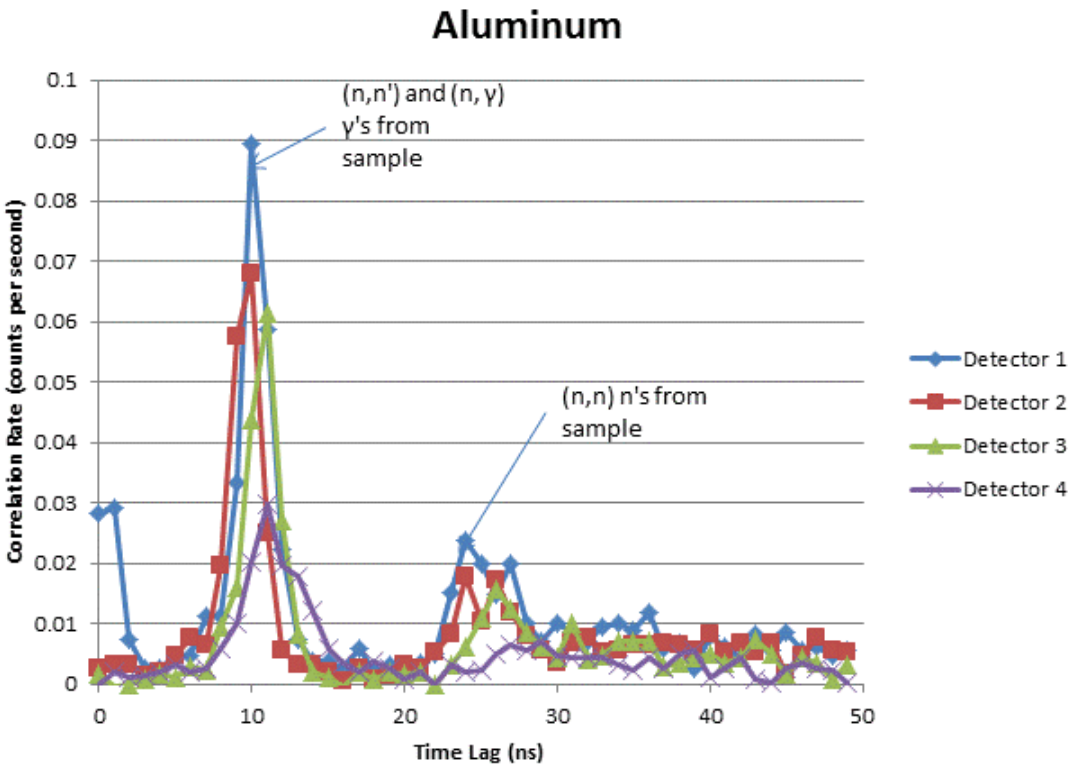

Fig. 7. Time-of-flight DT scattering measurement: aluminum.

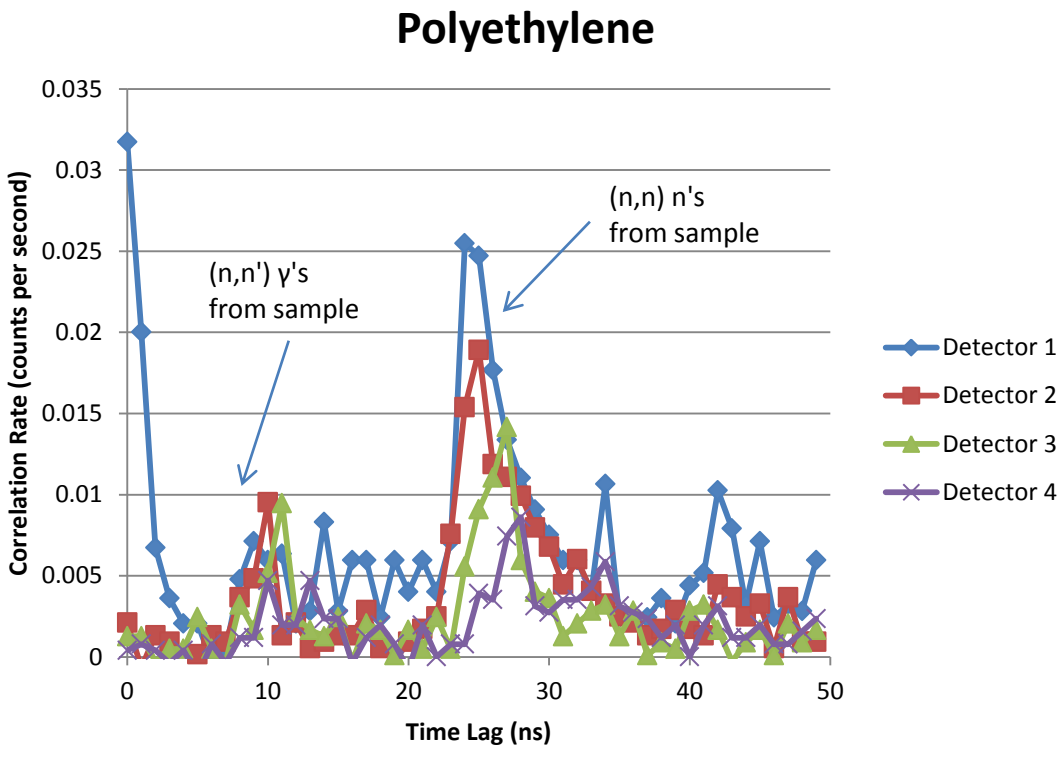

Fig. 8. Time-of-flight DT scattering measurement: polyethylene.

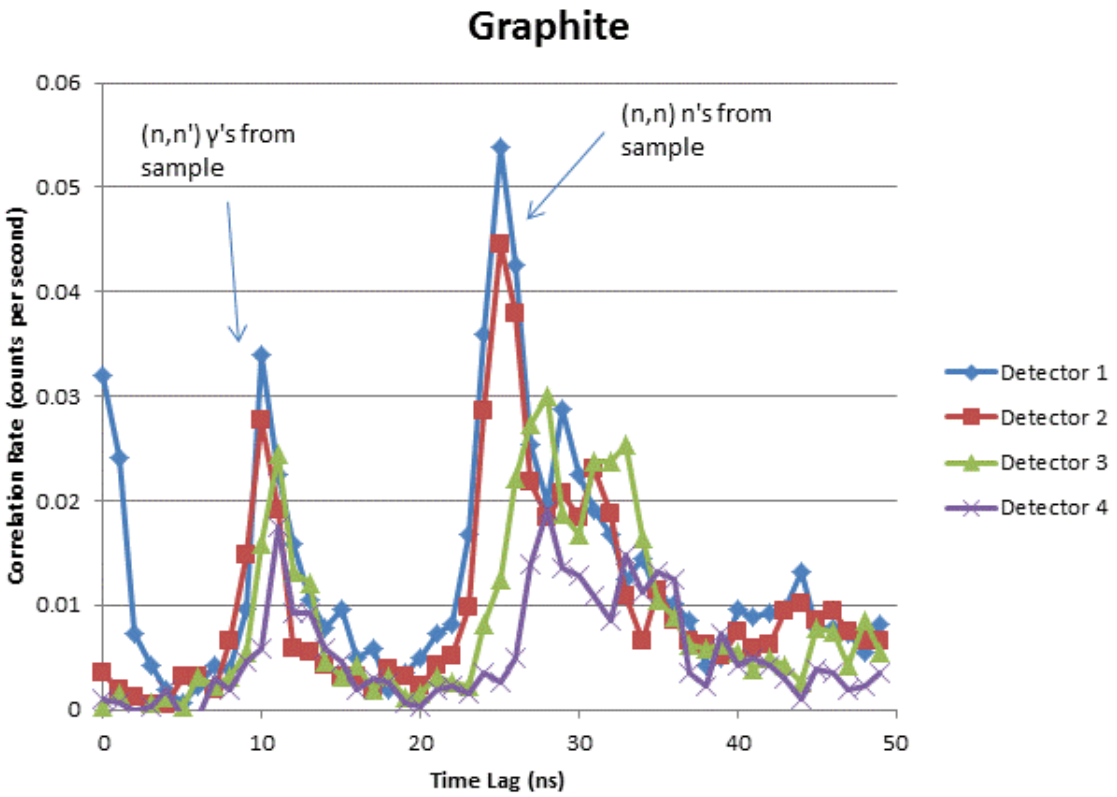

Fig. 9. Time-of-flight DT scattering measurement: graphite.

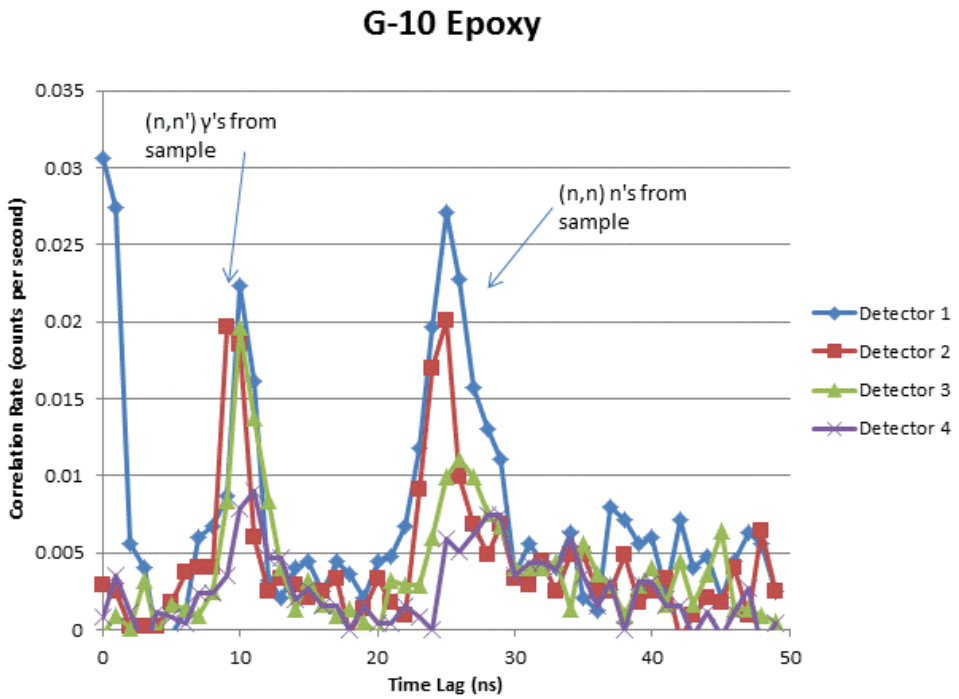

Fig. 10. Time-of-flight DT scattering measurement: G-10 Epoxy.

Aluminum produces far more gamma rays than graphite from non-elastic neutron scattering, because the aluminum's non-elastic neutron cross section at 14.1 MeV is 0.96 barns (ENDF/B-VII.1), while the

non-elastic cross section for carbon is only 0.53 barns (Ge et al., 2010). Polyethylene produces far fewer gamma rays than graphite because the nuclear density of carbon atoms in polyethylene is about half that of graphite (Table 2), and neutrons cannot scatter inelastically from the hydrogen in the material. After scattering from hydrogen nuclei, neutrons tend to be less energetic than the threshold energy for inelastic scattering in carbon, which also reduces the gamma-ray count.

The arrival times for neutrons in the G-10 measurement are consistent with those in polyethylene and graphite, which suggests that the largest nuclei in the G-10 sample are about the same mass as carbon. The height of the (n,n) peak in the G-10 measurement is similar to the height of the same peak in the polyethylene measurement, which indicates the presence of hydrogen in the sample. Gamma counts are more prevalent in the G-10 measurement than in the polyethylene measurement, which suggests that nitrogen may be present in the sample, since the threshold energy for inelastic neutron scattering is lower for nitrogen than for carbon.

In all four measurements, a peak appears near t = 0 for detector 1. This peak is due to gamma rays produced by non-elastic neutron interactions in the generator target and housing. These gamma rays were transmitted directly into detector 1, which was not entirely shielded from the generator by the tungsten block.

The neutron arrival times measured in the laboratory match very well with the expected values. Scattered neutrons from the aluminum sample arrived slightly earlier than scattered neutrons from the graphite sample, as predicted. The coincidence rate between elastically scattered neutrons and pixel 10 is also much lower for aluminum, relative to graphite, because aluminum tends to scatter more neutrons in the forward direction, instead of towards the scattering detector array. A comparison of the neutron arrival times in aluminum and graphite is shown in Fig. 11, and an MCNP-PoliMi (Pozzi, Padovani, and

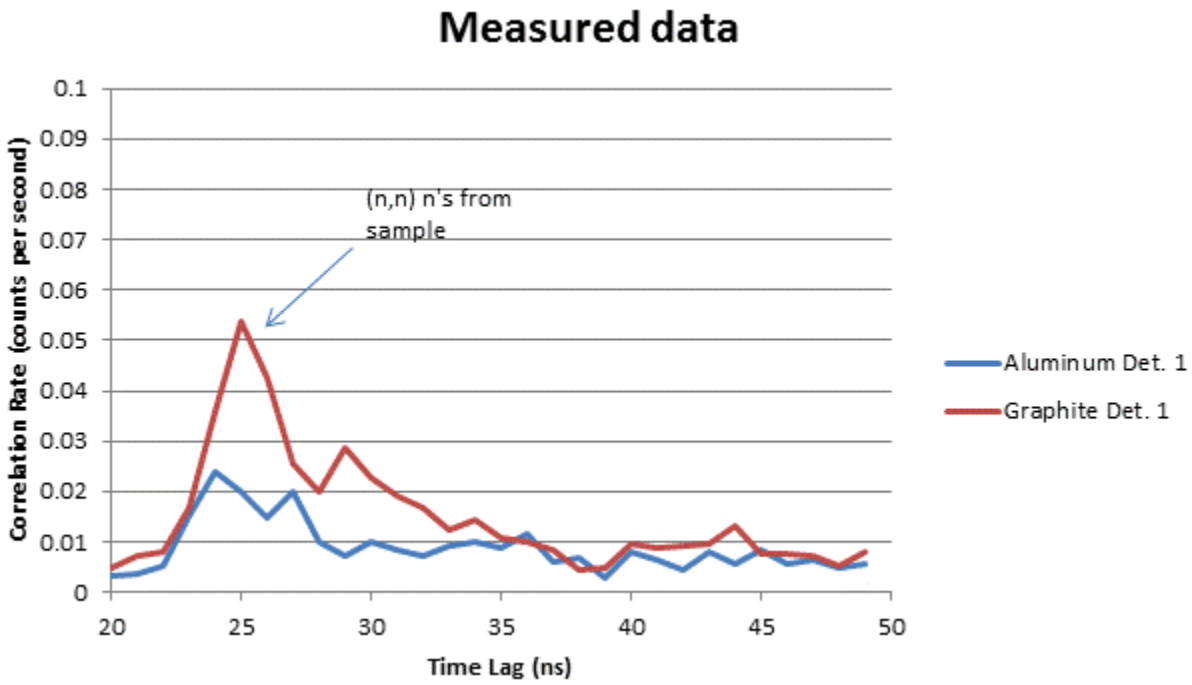

Fig. 11. Comparison between aluminum and graphite time-of-flight scattering measurements. Scattered neutrons from aluminum arrive slightly sooner because aluminum has a higher atomic mass.

Marseguerra, 2003) simulation of the same data is shown in Fig. 12. The measured and simulated data are very similar, and in both cases, the neutrons from the graphite sample arrive in the detector 1 ns after the neutrons from the aluminum sample.

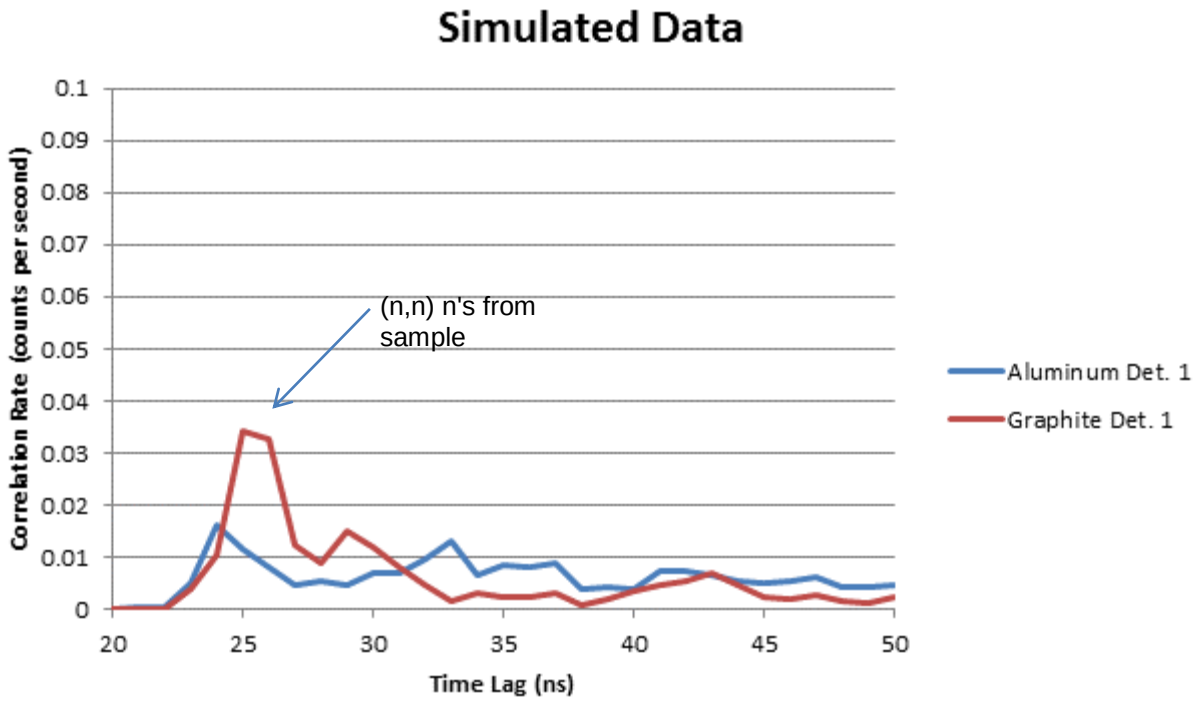

Fig. 12. Comparison between aluminum and graphite time-of-flight scattering simulations.

DT scattering measurements are useful for determining whether an unknown material contains high-Z or low-Z material, and whether a material contains large quantities of hydrogen. Neutrons scattering from heavy nuclei will arrive sooner in a detector than neutrons scattering from lighter nuclei. The presence of hydrogen tends to suppress the gamma counts in the scattering detectors, because it reduces the density of other nuclei in the material and its elastic scattering cross section is relatively large. Scattering measurements, however, are less useful for differentiating between nuclei such as ^{12}C, ^{14}N, and, ^{16}O, which have similar mass, since the energies of elastically scattered neutrons from each these target nuclei are very similar. Nevertheless, DT scattering measurements are a valuable tool, especially when complemented by NMIS's other capabilities.

5. CALIFORNIUM TRANSMISSION

In a californium transmission time-of-flight measurement, neutrons from a ^{252}Cf spontaneous fission source are transmitted through an unknown material. These measurements can assist in identifying a material by providing information about its neutron attenuation characteristics over the range of fission neutron energies (Mihalczo and Hill, 1971). Californium-252 transmission measurements of aluminum, polyethylene, graphite, and G10 epoxy samples are described in this section.

5.1 EXPERIMENTAL SETUP

The californium transmission measurements reported here used a setup similar to the apparatus used in the DT transmission measurement, except that a 0.3 mCi ^{252}Cf source on one plate of a parallel plate ion chamber detector was taped in front of the target spot on the DT generator. The center of the ^{252}Cf source

was horizontally level with the plastic scintillator array. The distance between the ^{252}Cf source and the detector array was 110 cm. Samples were placed parallel to the generator's long axis on a steel stand between the source and plastic scintillator detectors. The front face of each sample was 52 cm from the californium source. A picture of the setup is shown in Fig. 13, and the dimensions of the material samples are shown in Table 6.

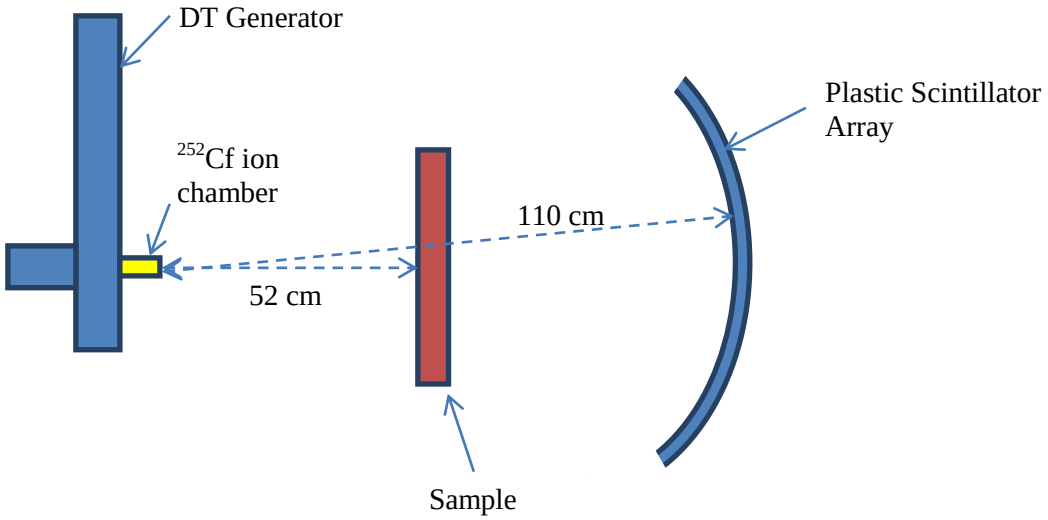

Fig. 13. Experimental setup for californium transmission measurements (not to scale).

Table 6. Dimensions of materials used in californium transmission measurements

Material	Dimensions (cm)
Polyethylene	30.5×30.5×7.6
Aluminum	30.5×30.5×7.6
Graphite	45.7×45.7×7.6
G-10	30.5×30.5×5.1

Signals from the ^{252}Cf ion chamber were processed through an ORTEC Model 935 CFD, and then sent to the NMIS processor. Coincidence counts between the californium source and the plastic scintillator array were collected in 42.7-minute-long measurements for each sample. The count rate in the californium source was approximately 175,000 counts/s in each measurement. Time-of-flight spectra between the californium source and detector 22 were measured for each material sample.

5.2 THEORY

Many nuclei have resonances in their neutron cross sections in the 0.2 MeV–6 MeV energy range, which characterizes most ^{252}Cf fission neutrons. Thus, the appearance of time-of-flight distributions for californium neutrons travelling through a particular material will depend upon variations in the material's nuclear cross section as a function of energy. An upward spike in a cross section at certain energies will

reduce counts at its corresponding location in the time-of-flight time coincidence distribution. Likewise, a downward spike will increase counts. Multiple neutron scattering and the time uncertainty of the plastic scintillator detectors, however, may reduce the appearance of these features in a time-of-flight spectrum.

The time-of-flight distributions for all four materials samples are predicted to be of interest because aluminum, carbon, and nitrogen display considerable variation over the energy range of the ^{252}Cf fission neutrons. Carbon is present in the graphite, polyethylene, and G-10 samples, and nitrogen may be present in the G-10 slab.

In order to confirm whether any features would be visible in a time-of-flight spectrum generated in the laboratory, an MCNP-PoliMi simulation with an aluminum sample was conducted using the same setup as the laboratory measurement, except with a 1-cm-thick slab. The simulation used 2×10^8 source particles. The time-of-flight distribution for neutrons incident on detector 16 is displayed in Fig. 14, along with the total microscopic cross section of aluminum across the energy range corresponding the neutron arrival times in the detector. The cross-section data were smoothed by averaging each data point over ±1 ns, to account for timing uncertainty in the neutron detectors. All cross-section data were obtained from the ENDF/B-VII.1 database.

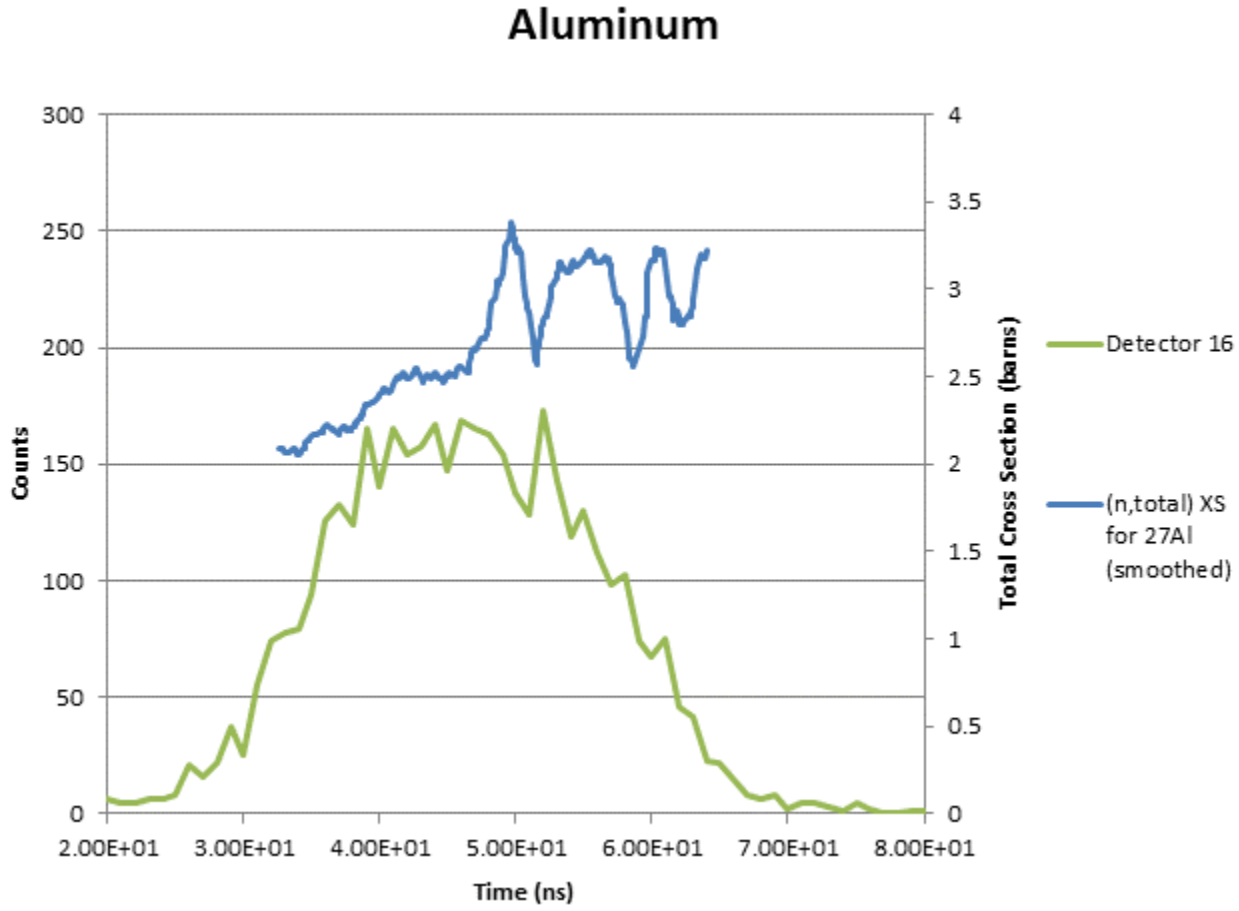

Fig. 14. Aluminum time-of-flight spectrum produced by MCNP-PoliMi, with the (n,total) cross section for the corresponding energies overlaid. Negative correlation is distinctly visible between the two data sets.

The time-of-flight spectrum shown in Fig. 14 clearly correlates with the cross-section data for ^{27}Al and therefore corroborated predictions that the features visible in the simulation results would be observable in laboratory data.

5.3 RESULTS

Time-of-flight spectra between the ^{252}Cf source and detector 22 are shown for aluminum, polyethylene, graphite, and G-10 epoxy in Figs. 15–18, respectively. Smoothed ^{27}Al cross-section data corresponding to neutron time-of-flight are shown in Fig. 15, unsmoothed ^{12}C cross-section data are shown in Figs. 16 and17, and unsmoothed ^{14}N cross-section data are shown in Fig. 18. Each point in the smoothed ^{27}Al cross-section data, as in Fig. 14, was averaged over ±1 ns to account for timing uncertainty in the plastic scintillator detectors. Simulated time-of-flight data from MCNP-PoliMi are also shown for the aluminum and polyethylene measurements.

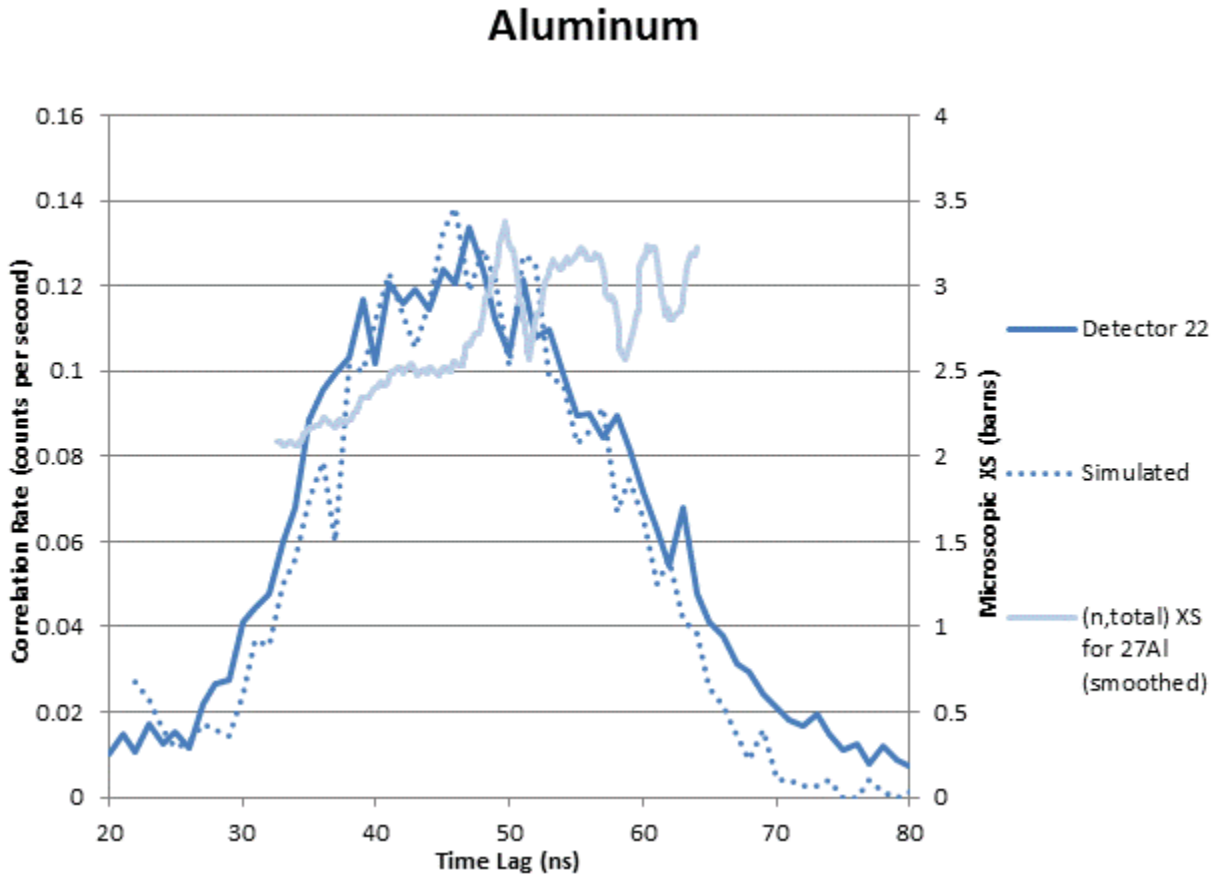

Fig. 15. Californium-252 fission neutron time-of-flight spectrum for aluminum sample with corresponding cross-section data. Simulated data compare well with measured data, and differences are probably due to neutrons scattering from other materials in the laboratory environment.

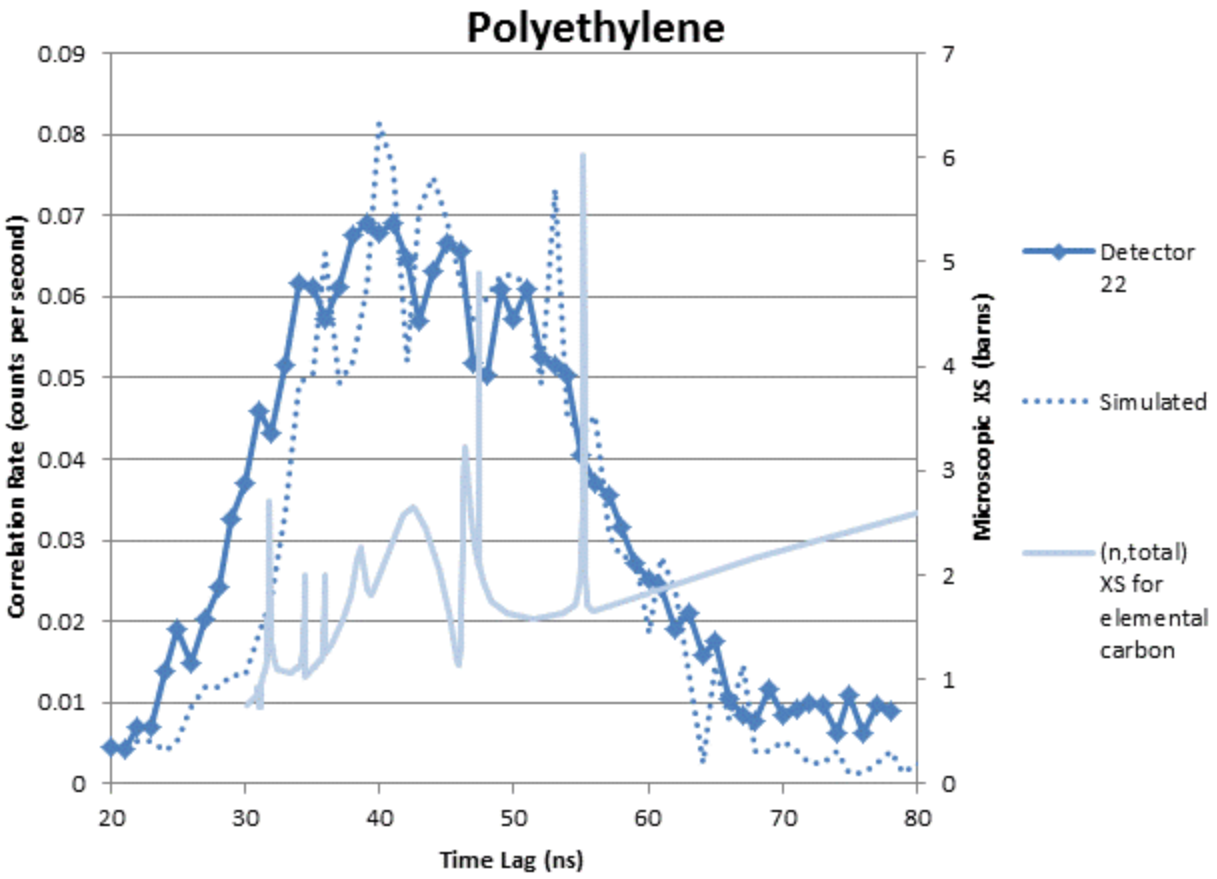

Fig. 16. Californium-252 fission neutron time-of-flight spectrum for polyethylene sample with corresponding cross-section data. The measured data and simulated data are similar, and as in the aluminum measurement, differences between the spectra are due to neutron scattering in ambient laboratory materials.

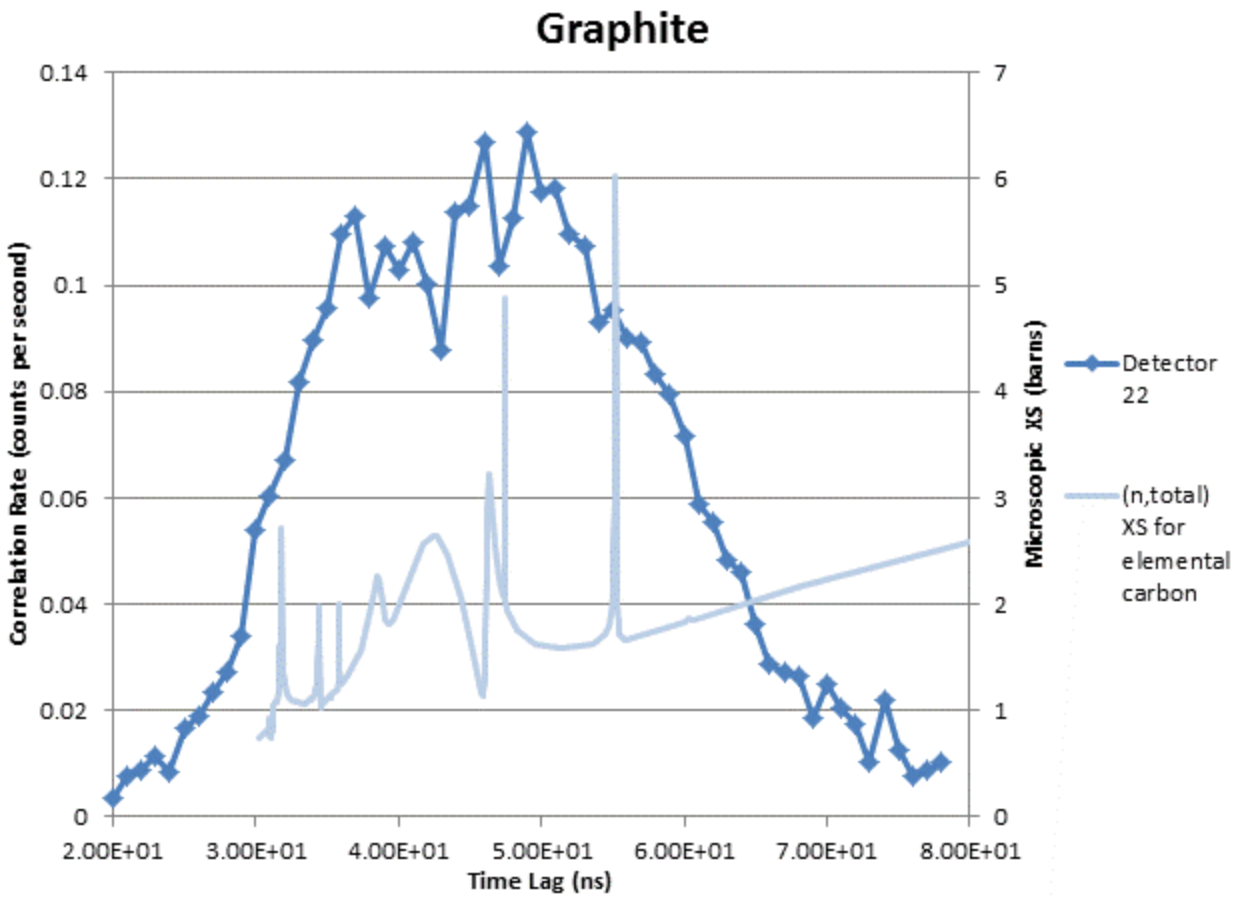

Fig. 17. Californium-252 fission neutron time-of-flight spectrum for graphite sample with corresponding cross-section data.

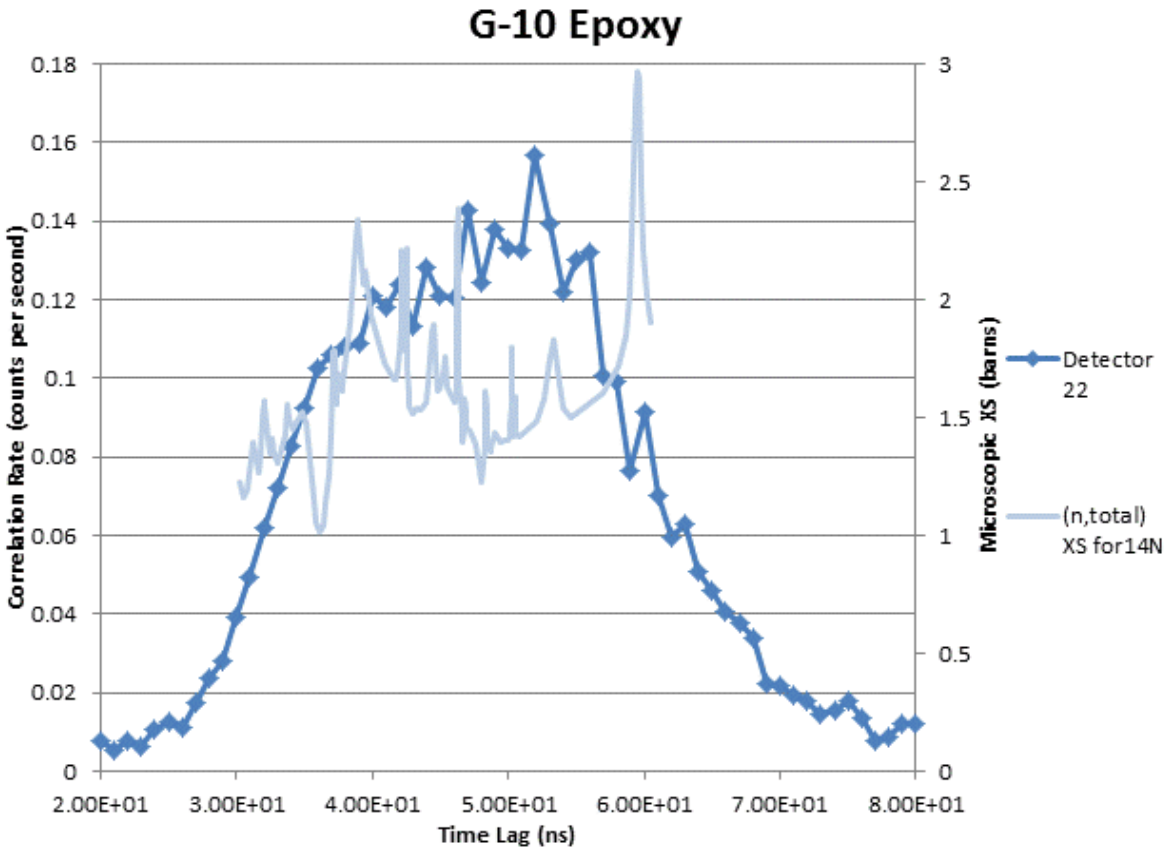

Fig. 18. Californium-252 fission neutron time-of-flight spectrum for G-10 epoxy sample with nitrogen cross-section data.

Strong negative correlations are visible in all four measurements between counts and neutron cross sections. The most obvious feature in the aluminum time-of-flight spectrum is a trough at ~50 ns that corresponds to a peak in the ^{27}Al cross section at the same arrival time. Overall, the aluminum spectrum matches well with the spectrum produced in the MCNP-PoliMi simulation.

The time-of-flight distributions for polyethylene and graphite also match well with carbon's cross sections over the same energy range. An important difference between the polyethylene and graphite data, however, is that graphite transmits neutrons at a much higher rate than polyethylene – the peak of the graphite distribution (Fig. 17) is approximately 0.13 counts/s, whereas the peak of the polyethylene curve is less than 0.07 counts/s. Polyethylene transmits fewer neutrons because it contains hydrogen, which stops neutrons far more efficiently than carbon.

The G-10 epoxy time-of-flight curve agrees well with cross-section data for ^{14}N. The diminished count rates on the left-hand side of the neutron distribution (between 40 and 50 ns) correspond with a rise in the ^{14}N total neutron cross section over the corresponding energy range.

The data gathered in all four measurements demonstrates that neutron cross-section behavior can be inferred from neutron time-of-flight measurements of ^{252}Cf fission neutrons through a material. This cross-section information can then be used to identify unknown materials if it is compared to a library of known cross-section data for different nuclei over the range of approximately 1 MeV–7 MeV. Californium transmission measurements are a valuable tool in material identification, because they provide data on a material's neutron cross section over a fission spectrum of energies.

6. ACTIVE GAMMA SPECTROSCOPY

Measurements of characteristic gamma emissions resulting from non-elastic neutron interactions can be used to identify materials with low-to-medium nuclear mass, and may be particularly useful for identifying explosives or drugs inside shielded packages. This section presents results of active gamma spectroscopy measurements with NMIS.

6.1 MCNP-PoliMi SIMULATION

Prior to measurements being made in the laboratory, MCNP-PoliMi simulations were performed in a setting with no surrounding material effects to evaluate the prospects of detecting gamma rays originating from non-elastic neutron reactions. The simulations included a 14.1 MeV neutron source, a 30.5×30.5×7.6-cm slab of material, and a 10.2×10.2×40.6-cm sodium iodide scintillator in the arrangement shown in Figs. 19 and 20. One simulation was performed with aluminum as the material, and another with polyethylene. Each simulation contained 1×10^7 source particles.

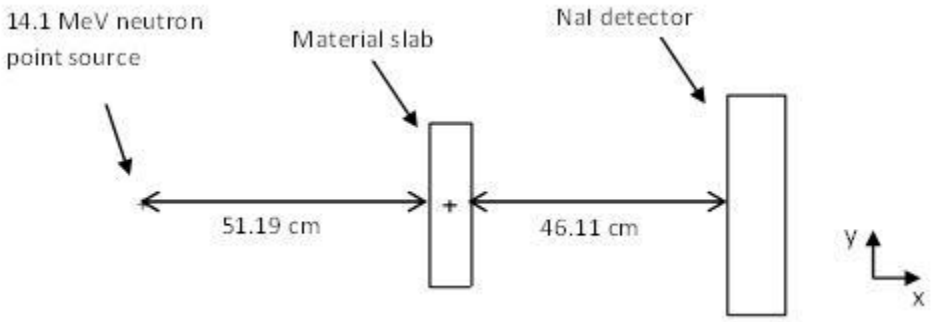

Fig. 19. MCNP-PoliMi input visualization.

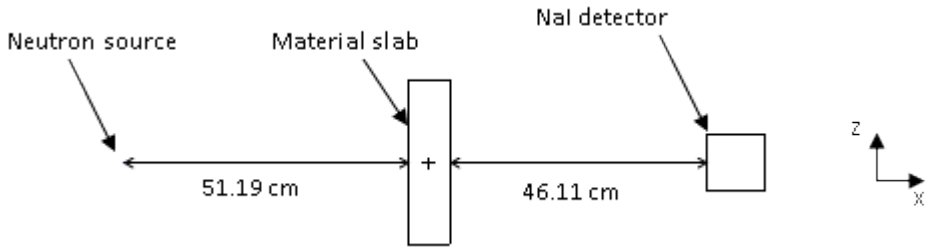

Fig. 20. MCNP-PoliMi input visualization.

Both simulations were post-processed using PolimiPP software (Grogan, 2010), which recorded the energy deposited in the NaI detector by each photon that could be correlated with a source neutron. Photon peaks are visible from both simulations, and it is visibly apparent that the gamma spectra for the two different materials are very different. For the polyethylene simulation, a very large peak at 4.44 MeV represents the first excitation level of the ^{12}C nucleus. A single escape peak for this gamma is also visible. Photon deexcitations are also visible for the ^{27}Al nucleus, resulting from both inelastic neutron scattering and neutron absorption. A gamma emission is also visible from the decay of ^{28}Al, which follows on after neutron absorption in ^{27}Al. The vastly different spectra produced by these simulations, shown in Fig. 21, gave a very good indication that similar gamma spectra could be measured and differentiated in the laboratory.

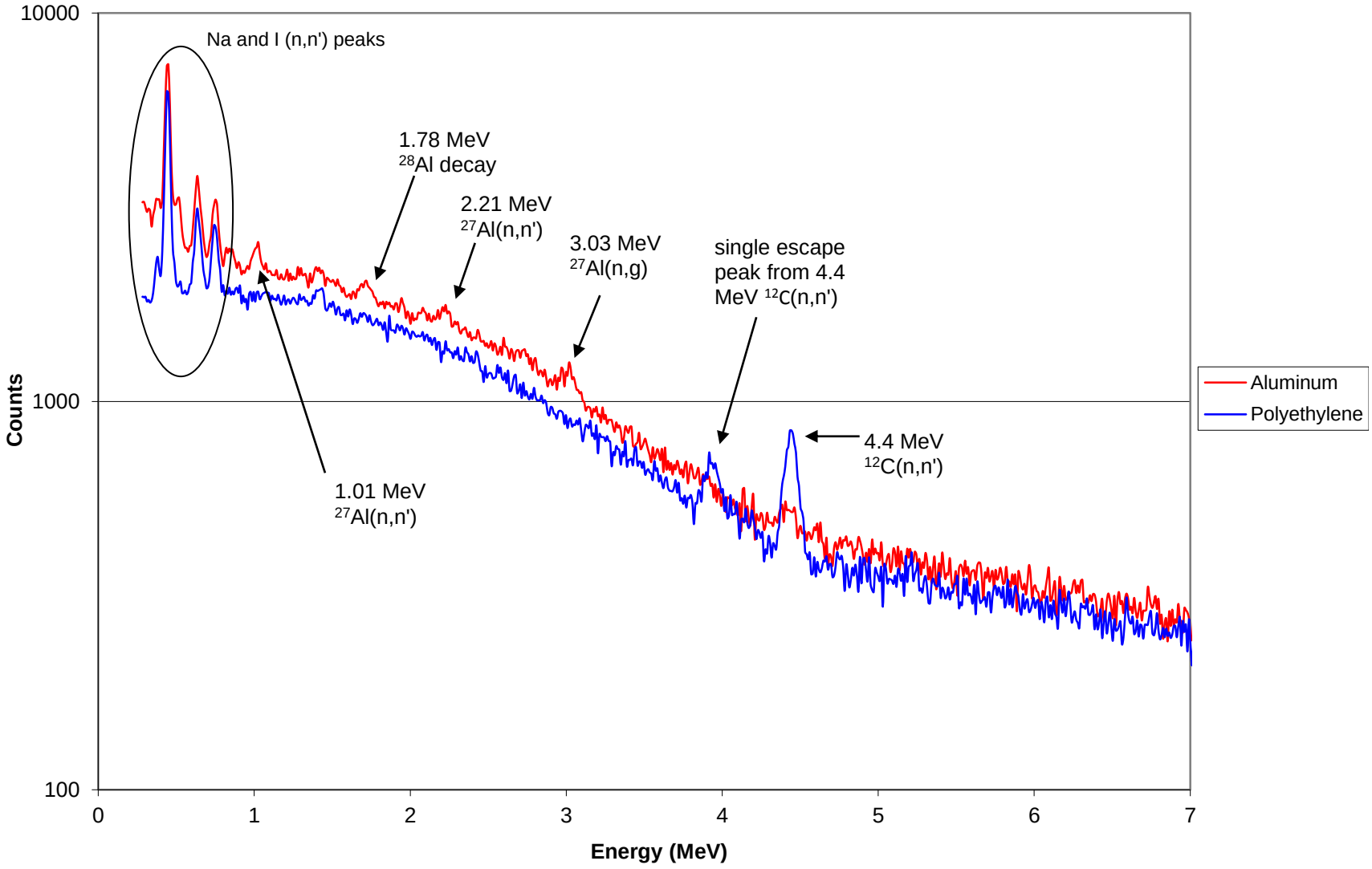

Fig. 21. Gamma spectrum from simulation result for 14.1 MeV neutrons on aluminum and polyethylene. Energy peaks are matched with nuclear level data from Nuclear Data Sheets (Basunia, 2011).

6.2 EXPERIMENTAL SETUP

The apparatus used for active gamma spectroscopy measurements with NMIS was slightly different from the setup used for DT transmission measurements. The DT generator was used as a neutron source, but a single-pixel, 5-cm-diameter PMT (ORTEC model 265) was used for neutron tagging. With the new PMT in place, tagged neutrons were subtended by a 45° cone, with the long axis along the centerline between the neutron generator and plastic scintillator array. Material samples were placed at a 45° angle, with the front face of each sample positioned 42 cm away from the neutron generator's target spot. A 10.2×10.2×40.6-cm NaI(Tl) detector (Alpha Spectra Model 16D16X64 3.5) was placed so that the center of its front face was 61 cm away from the center of the face of the material sample. The center points of the generator, sample, and detector were level on a horizontal plane. An ORTEC model 276 PMT was coupled to the detector. This arrangement, shown in Figs. 22 and 23, was designed in order to maximize the number of neutrons incident on the material slab, and to maximize the number of photons counted in the NaI detector, while minimizing the number of neutrons incident on the detector and keeping detector dead time reasonably low. The NaI detector's PMT was supplied with a potential of +925 V, and the PMT for the alpha detector was supplied with -2121 V.

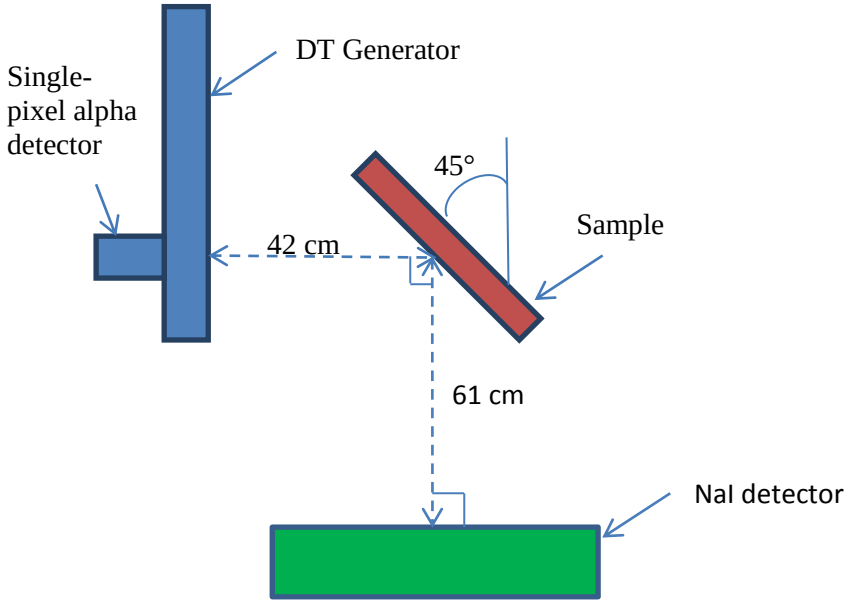

Fig. 22. Experimental setup for active gamma spectroscopy measurements.

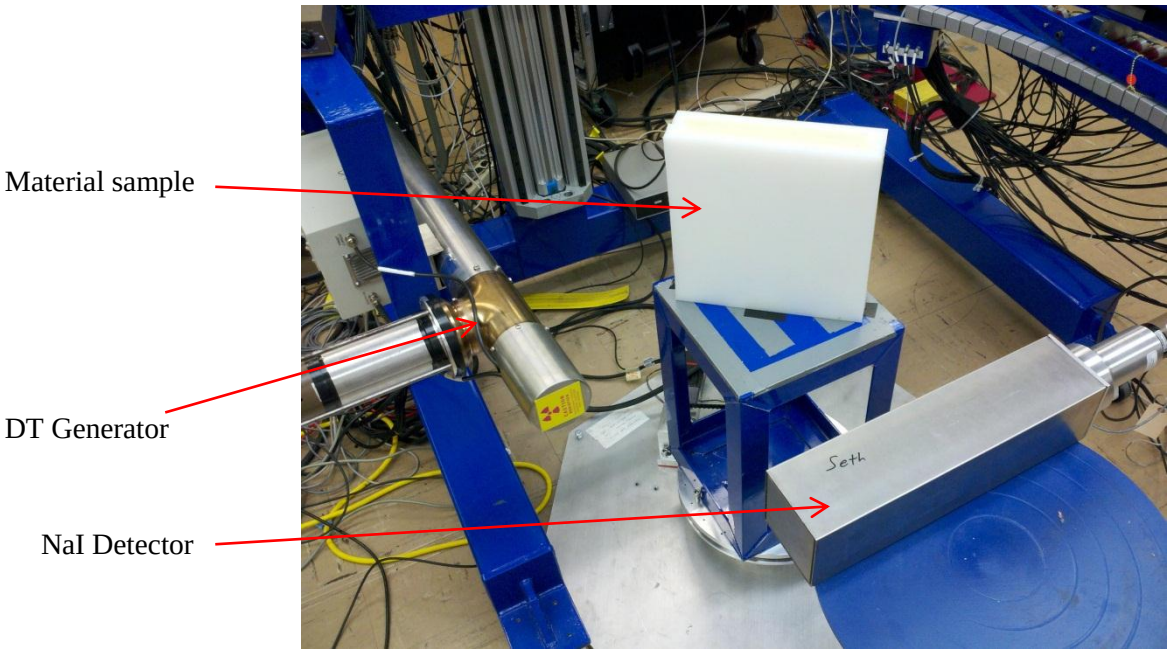

Fig. 23. Setup for active gamma spectroscopy measurements.

A coincidence circuit was constructed in an ORTEC 4001C NIM bin so that only photons correlated with a source neutron would be counted. The signals of both the neutron generator's alpha detector and the NaI detector were sent to CFD modules, each with a trigger delay corresponding to the rise time of the anode pulse. Logic pulses from the alpha detector were delayed further by 75.5 ns so they would arrive at the same time as their corresponding pulses from the NaI detector. When an alpha and gamma pulses arrived in coincidence, a 5 μs timing gate was sent to a multi-channel analyzer (MCA), where the height of the NaI detector's energy pulse was recorded. A schematic of this circuit is shown in the Fig. 24. Each measurement used 1800 s of live time in the MCA, with the DT Generator running at 25 μA of beam current and a voltage of 75 kV. Approximately 2×10^5 neutrons/s were tagged by the alpha detector. The pulse height distribution for the alpha detector, clearly displaying a monoenergetic distribution of alpha particles, is displayed in Fig. 25.

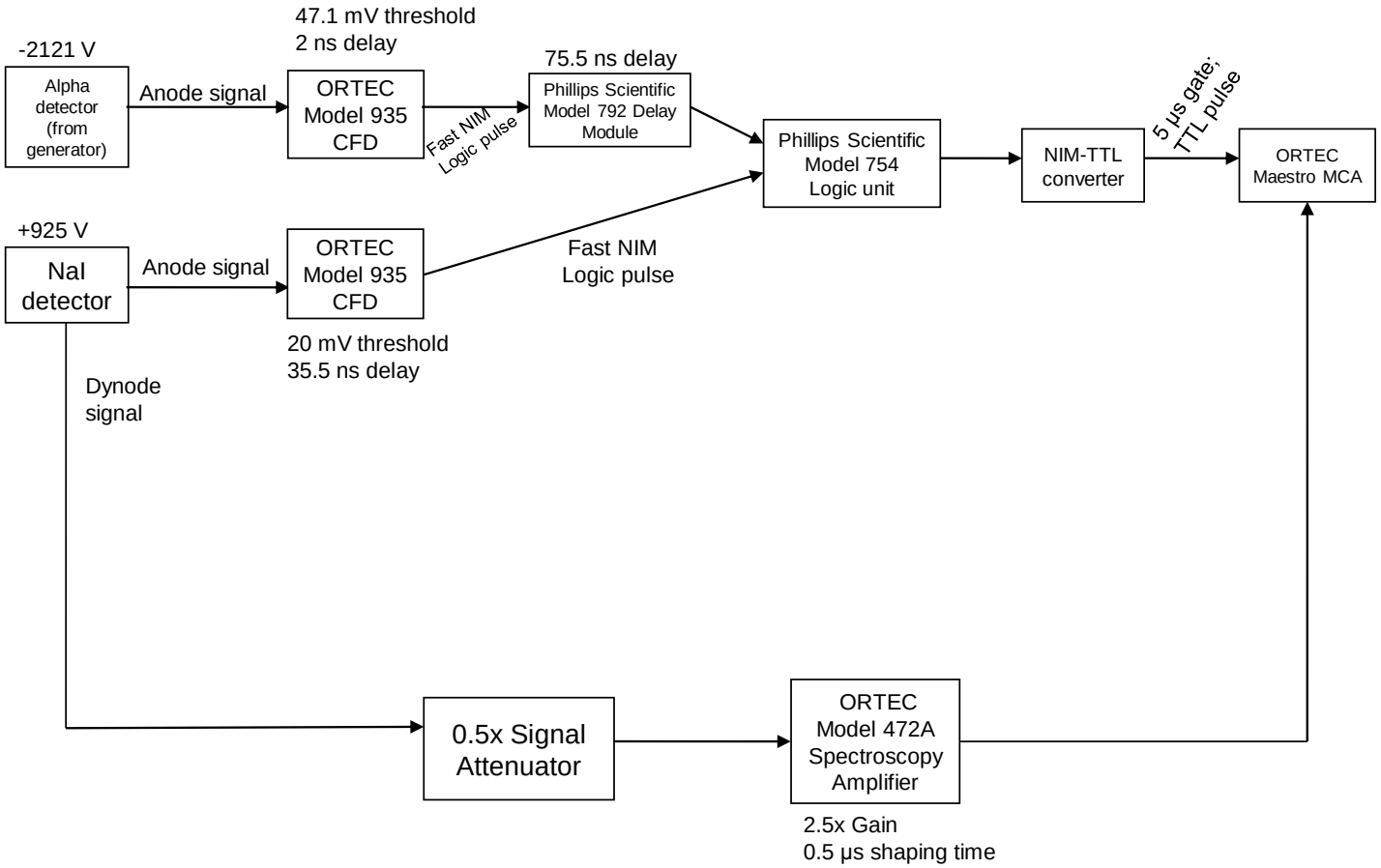

Fig. 24. Schematic of coincidence system used for active gamma spectroscopy measurements.

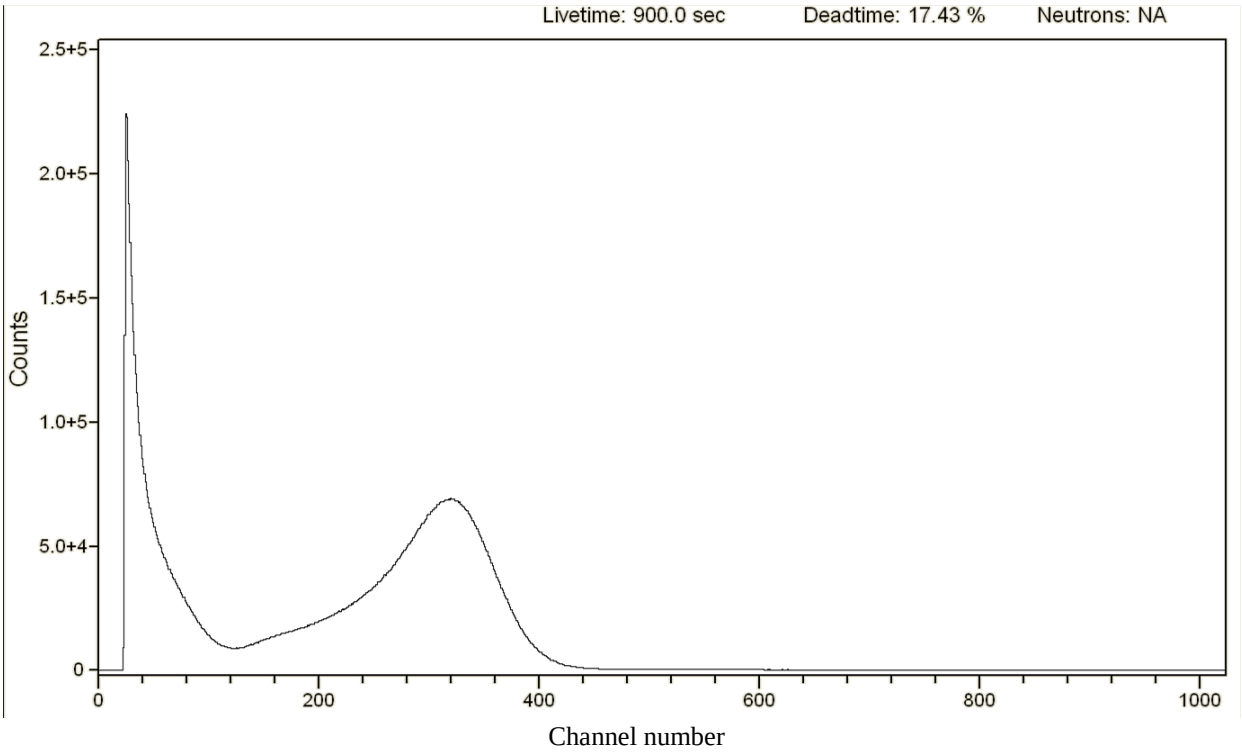

Fig. 25. Pulse height distribution for single-pixel alpha detector.

The dimensions of the material samples used in the active gamma spectroscopy measurements are shown in Table 7.

Table 7. Dimensions of material samples used for active gamma spectroscopy measurements

Material	Dimensions (cm)
Polyethylene	30.5×30.5×7.6
Aluminum	30.5×30.5×7.6
Graphite	45.7×45.7×7.6
G-10	30.5×30.5×5.1

6.3 RESULTS

Data from each material measurement was used to produce a pulse height spectrum for counts in the NaI detector coincident with counts in the neutron generator. Another pulse height spectrum was produced for a measurement with no sample present. This spectrum was subtracted from each material's spectrum, in order to compensate for the effects of neutrons incident on the detector, as well as non-elastic neutron interactions inside the detector. Spectra for aluminum, polyethylene, graphite, and G-10 epoxy are shown in Figs. 26, 27, 28, and 29, respectively. Pulse height analysis was conducted with Los Alamos National Laboratory's PeakEasy software.

Aluminum

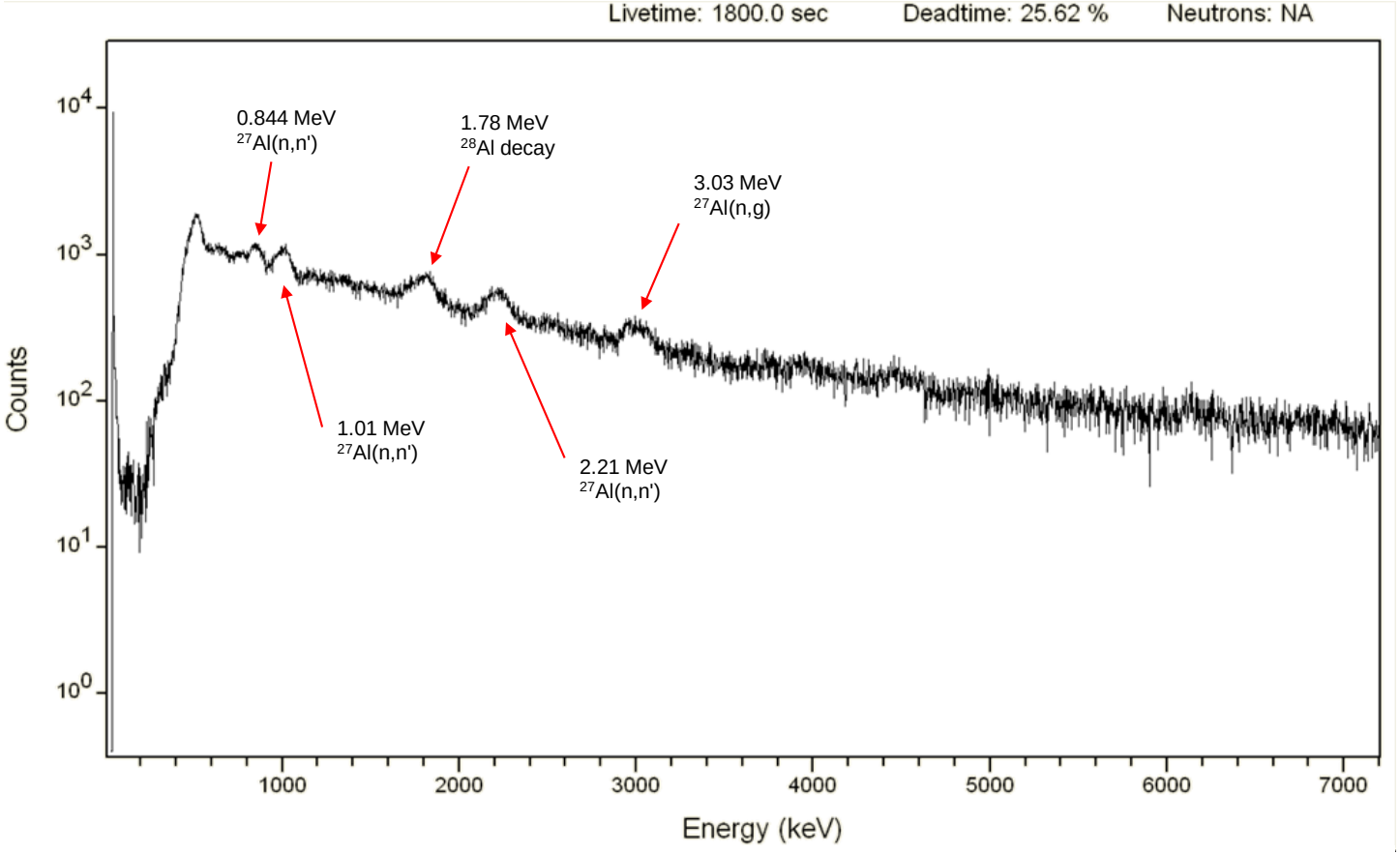

Fig. 26. Gamma-ray spectrum from aluminum measurement. This spectrum is very similar in appearance to the simulated spectrum shown in Fig. 21.

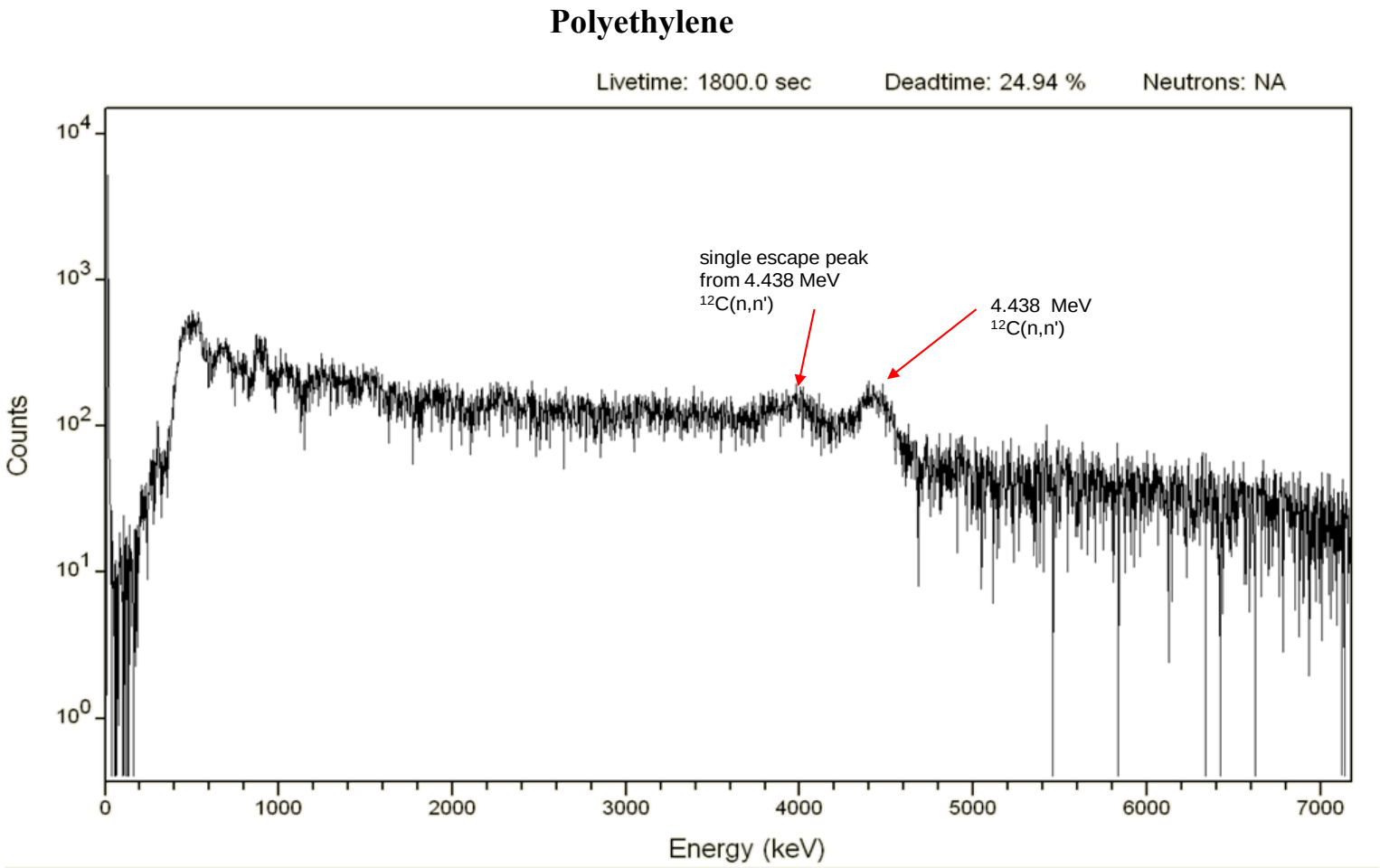

Fig. 27. Gamma-ray spectrum from polyethylene measurement. A 4.44 MeV full-energy peak, as well as a 3.9 MeV single escape peak are visible, as in the simulation shown in Fig. 21.

Graphite

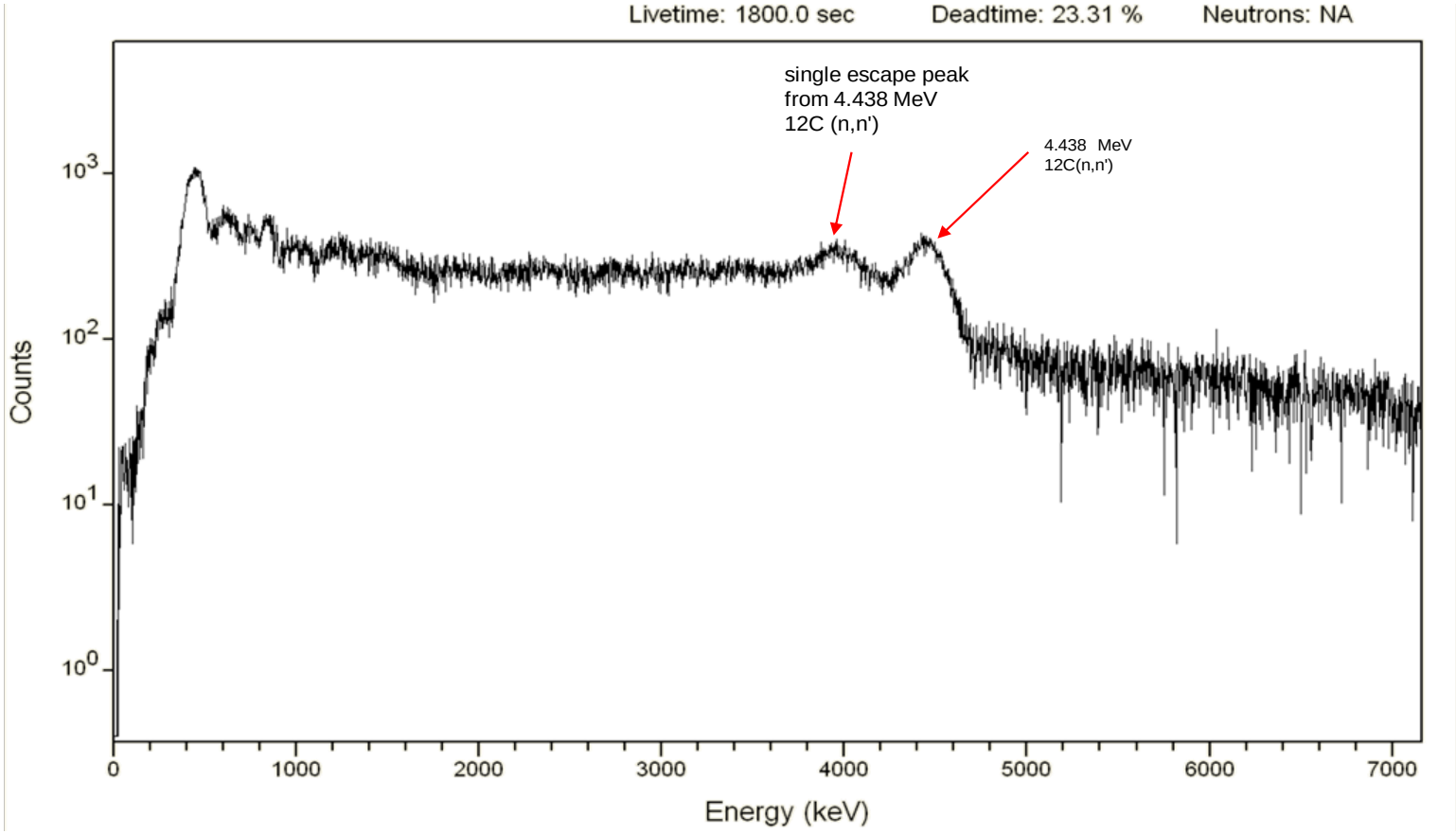

Fig. 28. Gamma-ray spectrum from graphite measurement.

G-10 Epoxy

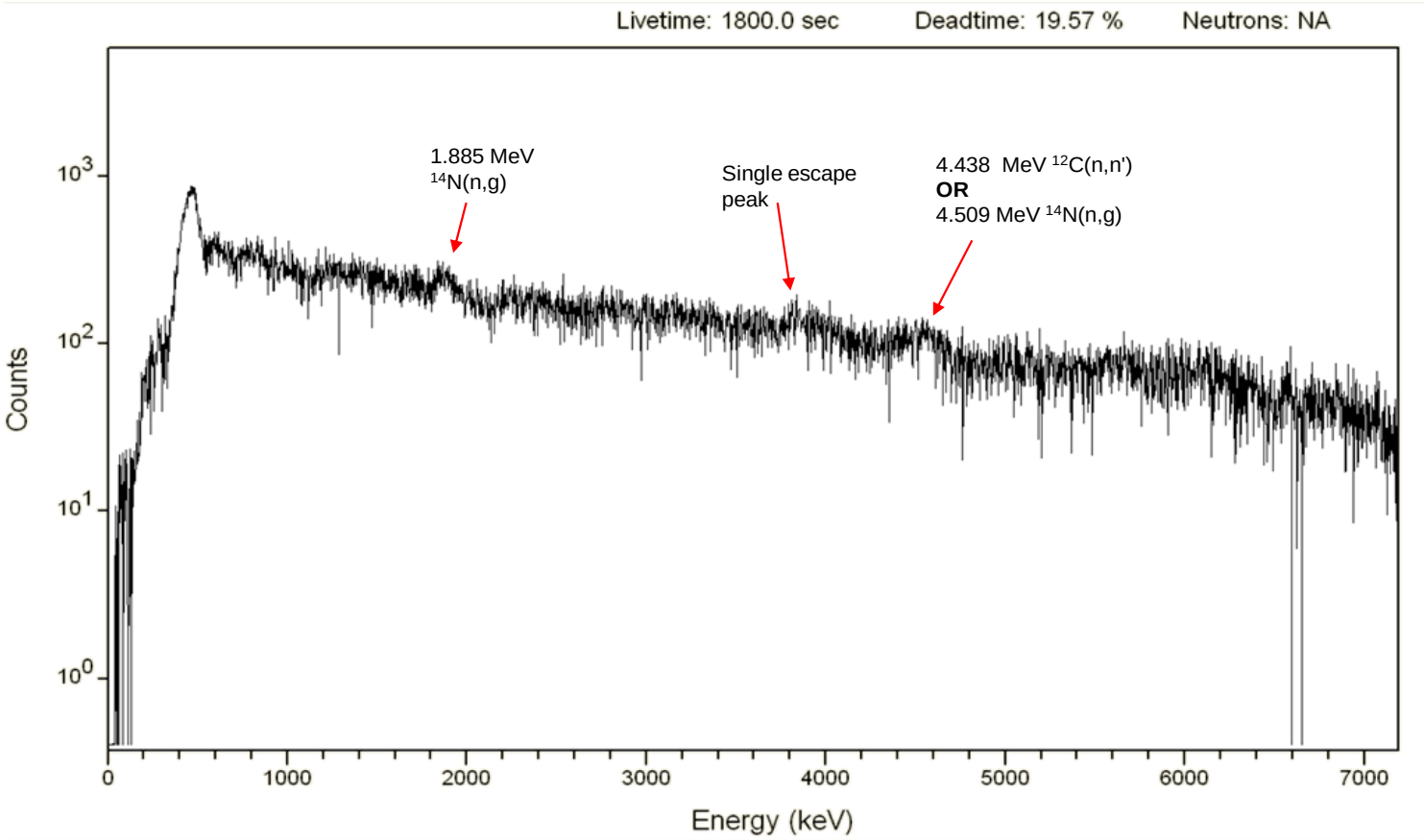

Fig. 29. Gamma-ray spectrum from G-10 epoxy measurement.

In the aluminum measurement, strong ^{27}Al inelastic scattering peaks are found at 0.844 MeV, 1.01 MeV, and 3.03 MeV. The spectrum also contains evidence that some neutrons were captured in the aluminum slab, since a 3.03 MeV capture line is clearly visible, along with a 1.78 MeV photon emission from the decay of ^{28}Al. These results are in agreement with the spectrum predicted in the simulations, and clearly signify that the material being measured was aluminum.

A 4.44 MeV peak is clearly visible in the carbon spectrum, which represents the first nuclear excitation level of ^{12}C, indicating that the material being measured is indeed carbon. A single-escape peak for the 4.44 MeV gamma is also present. Even though polyethylene contains hydrogen, a hydrogen capture peak is not visible in this spectrum. This could be due to a high rate of neutron incidence in the detector. Fast neutrons produce a background energy spectrum in NaI detectors that is similar to an exponential decay function (Knoll, 2011). Lower energies receive far more counts than higher energies, and at 2.2 MeV, the number of hydrogen capture gammas detected were not high enough to register above the neutron background. Even though this effect was partly reduced by subtracting out a spectrum with no object present, fast-neutron detector effects are still visible in the spectra presented.

In the graphite measurement, the 4.44 MeV peak is slightly more pronounced than in the polyethylene measurement. This is because the graphite slab, at 45.7×45.7×7.6 cm., is larger than the 30.5×30.5×7.6-cm. polyethylene slab. The graphite slab also has a higher nuclear density, which would account for more inelastic scattering interactions in the graphite slab. Also, the nuclear density of carbon in the graphite slab is higher, which would increase further the production of 4.44 MeV photons. Apart from the sizes of the 4.44 MeV peaks, the spectra produced by graphite and polyethylene are very similar. Slightly less noise appears in the graphite measurement because the slab's larger size attenuated more neutrons, preventing them interacting with other objects in the laboratory.

While the nitrogen nuclei in G10 epoxy were not appreciably excited through inelastic scattering, a 1.885 MeV neutron absorption peak was detected, which implies the presence of ^{14}N in the material. Another peak was detected in the region of 4.4–4.5 MeV with a corresponding single escape peak. This broad peak could be attributed to either inelastic neutron scattering in ^{12}C nuclei (4.44 MeV), or to neutron absorption in ^{14}N (4.509 MeV). Since both carbon and nitrogen are found in G10 epoxy, it is difficult to determine which element contributed more to the peak. Nevertheless, the 1.885 MeV nitrogen absorption peak clearly indicates the presence of nitrogen.

Active gamma spectroscopy has proven to be a useful technique that is compatible with the NMIS system. Laboratory measurements enabled differentiation between aluminum and polyethylene, and if developed further, may allow differentiation between organic materials. Future gamma spectroscopy measurements could be improved, however. Energy resolution in the sodium iodide detector is poor. Resolution could be enhanced by using a high-purity germanium detector in a future measurement. The germanium detector would have to be shielded from neutron flux with a tungsten block (as used in the DT scattering measurements) to prevent its crystal structure from being damaged. Even if a sodium iodide detector is used in a future measurement, it should still be shielded from neutrons, which produce unwanted background counts in the detector. In the future, active gamma spectroscopy may evolve into a robust identification technique for unknown materials with low nuclear mass.

7. CONCLUSIONS

This report demonstrated the applicability of four different measurement techniques that can be used in conjunction with NMIS fast-neutron imaging, including the mapping of fission sites for identifying unknown materials. These methods often complement each other: active gamma spectroscopy, for example, can be useful for differentiating between materials with similar nuclear mass, which would limit the effectiveness of a DT scattering measurement. The data collected from the DT transmission, DT

scattering, and californium transmission measurements behaved as predicted. The results of the active gamma spectroscopy measurements demonstrate the viability of the addition of a gamma spectroscopy module to a future version of NMIS. Adding active gamma spectroscopy to complement NMIS time coincidence data will deepen the versatility of the system's capabilities and may aid in NMIS's ability to detect explosives, drugs, or other nonradiological materials.

8. REFERENCES

Basunia, M. S., " Nuclear Data Sheets 112," 1875 (2011).

Chadwick, M. B., M. Herman, et al., "ENDF/B-VII.1 Nuclear Data for Science and Technology: Cross Sections, Covariances, Fission Product Yields and Decay Data," *Nuclear Data Sheets*, **112**, pp. 2887–2996, (2011).

Chiang, L. G., A. C. Gehl, J. K. Mattingly, J. A. McEvers, J. T. Mihalczo, J. A. Mullens, and R. B. Oberer, *"Nuclear Materials Identification System Operations Manual*," Technical Report, ORNL/TM-2001/65, Oak Ridge National Laboratory, (2001).

Duderstadt, J. J., and L. J. Hamilton, *Nuclear Reactor Analysis*, Wiley, New York, (1976).

Ge, Z. G., Ge, Y. X. Zhuang, et al., "The Updated Version of Chinese Evaluated Nuclear Data Library (CENDL-3.1),", *Proceedings of the International Conference on Nuclear Data for Science and Technology*, Jeju Island, Korea, April 26–30, 2010.

Grogan, B. R., " Grogan, "The Development of a Parameterized Scatter Removal Algorithm for Nuclear Materials Identification System Imaging,"" PhD dissertation., University of Tennessee, (2010).

Grogan, B. R., S. M. McConchie, J. T. Mihalczo, and J. A. Mullens, "Measurements of 14.1 MeV Neutron Reflection and Transmission for Carbon, Polyethylene, and Steel," *International Conference on the Physics of Reactors*, Interlaken, Switzerland, 2008.

Hausladen, P. A. Hausladen, J. T. Mihalczo, P. R. Bingham, J. A. Mullens, and J. S. Neal, "Enhanced Nuclear Materials Control and Accountability by Imaging," *Proceedings of the INMM 47th Annual Meeting,* Institute of Nuclear Materials Management, 2006.

Hurley, P., and J. Tinsley, *"Microchannel plate for position sensitive alpha particle detection*," Technical Report, DOE/NV/25946--152, U.S. Department of Energy, (2007).

Knoll, G. F., *Knoll, "Radiation Detection and Measurement*," 4th ed., Wiley, (2011).

Mattingly, J. K., T. E. Valentine, and J. T. Mihalczo, *"Use of the Nuclear Materials Identification System (NMIS) for Enhanced Receipt Confirmation Measurements at the Oak Ridge Y-12 Plant*", Technical Report, Y/LB-16,025, Oak Ridge Y-12 Plant, (2000).

McConchie, S. M., P. A. Hausladen, J. T. Mihalczo, B. W. Blackburn and D. L. Chichester, "Pulsed D-D Neutron Generator Measurements of HEU Oxide Fuel Pins," *AIP Conference Proceedings*, **1099**, pp. 643–646, (2009).

Mihalczo, J .T., *"Radiation Detection from Fission*," Technical Report, ORNL/TM-2004/234, (Oak Ridge National Laboratory, 2004).

Mihalczo, J. T., and N. W. Hill, "Simple Time-of-Flight Transmission Measurement for Incorporation in Nuclear Engineering Curricula," *Transactions of the American Nuclear Society,* **14** (1), pp. 60–61, (1971).

Mihalczo, J. T., et al. "Physical description of nuclear materials identification system (NMIS) signatures," *Nuclear Instruments and Methods in Physics Research Section A*, **450**, pp. 513–555, (2000).

Mihalczo, J. T., J. K. Mattingly, J. S. Neal, and J. A. Mullens, "NMIS plus gamma spectroscopy for attributes of HEU, PU and HE detection," *Nuclear Instruments and Methods in Physics Research Section B*, **213**, pp. 378–384, (2004).

Mullens, J. A. Mullens, J. T. Mihalczo, and P. R. Bingham, "Neutron and Gamma Ray Imaging for Nuclear Materials Identification," *Proceedings of the INMM 45th Annual Meeting*, Institute of Nuclear Materials Management, 2004.

Pozzi, S. A., E. Padovani, and M. Marseguerra, "MCNP-PoliMi: a Monte-Carlo code for correlation measurements," *Nuclear Instruments and Methods in Physics Research Section A*, **513**, pp. 550–558, (2003).

Pozzi, S. A., J. T. Mihalczo, P. Peerani, J. Loeschner, L. Cartegni, J. A. Mullens, and P. A. Hausladen, "Passive (NMIS) Meaasurements on Plutonium Oxide Samples," *Proceedings of the INMM 46th Annual Meeting*, Institute of Nuclear Materials Management, 2005.

Radle, J. E., D. E. Archer, J. A. Mullens, J. T. Mihalczo, C. L. Britton, Jr., R. F. Lind, M. C. Wright, and C. R. Brittain, "Fieldable Nuclear Material Identification System," *Proceedings of the INMM 50th Annual Meeting,* Institute of Nuclear Materials Management, 2009.

Smith, A. B., P. R. Fields, and J. H. Roberts, "Spontaneous Fission Neutron Spectrum of Cf^{252}," *Physical Review*, **108**, pp. 411–413, (1957).